PHOSWICH BETA-GAMMA SPECTROSCOPY

by

Allen Eugene Moon
B.S., Kansas State University, 1985

A MASTER'S THESIS

submitted in partial fulfillment of the
requirements for the degree

MASTER OF SCIENCE

Department of Nuclear Engineering
KANSAS STATE UNIVERSITY
Manhattan, Kansas

1987

Approved:

Major Professor

TABLE OF CONTENTS

		Page
I.	INTRODUCTION.	1
II.	PHOSWICH DETECTOR PULSE SHAPE ANALYSIS.	6
	A. Time Dependent Scintillation Current.	8
	1. Radiation Energy Absorbed in Each Scintillator	10
	2. Phoswich Detector Scintillator Current. . .	12
	B. Voltage Pulses from the PMT	14
	C. Voltage Pulses from PSD Circuit Components. . .	19
	1. Delay Line Shaping.	21
	2. CR Differentiation and RC Integration . . .	23
	3. Single Differentiation of PMT Voltage Pulse	27
	4. Double Differentiation of PMT Voltage Pulse	32
	5. Single Integration of PMT Voltage Pulse	41
	6. Differentiation and Integration of PMT Voltage Pulse	47
III.	PHOSWICH DETECTOR ASSEMBLY.	58
	A. Plastic Scintillators	58
	B. Wratten Gel Optical Filters	63
	C. Photomultiplier Tube Characteristics.	64
	1. PMT Electron Current Pulse.	64
	2. Relative PMT Charge	66
	D. Detector Assembly Overall Sensitivity	68
	1. Maximum Gamma-Ray Discrimination Ratio. . .	70
	2. Optimum Total Thickness of the Phoswich Detector	72
	3. Energy Nonlinearity	74
	E. Construction of KSU Phoswich Detector Assemblies.	75
IV.	PHOSWICH BETA-GAMMA SPECTROMETER SYSTEMS.	79
	A. Theoretical Pulse Shaping Amplifier Waveforms	80
	1. Linear Spectroscopy Amplifier	82
	2. Delay Line Shaping Amplifier.	84
	3. Timing Filter Amplifier	88
	B. Zero Crossing Time Associated Electronics . . .	92
	C. Pulse Shape Analyzer.	95
	D. Pulse Shape Discrimination Timing	99

Page

V. RESULTS AND CONCLUSIONS 106
A. Characteristic Time Constants of the Scintillators and PMT 111
B. Relative PMT Charge for Scintillator and Filter Combinations 112
C. Linear Spectroscopy Amplifier Voltage Waveform. 116
D. Delay Line Shaping Amplifier Voltage Waveform. 116
E. General Observations of the Voltage Waveforms 121

VI. SUGGESTIONS FOR FURTHER STUDY 123

VII. ACKNOWLEDGEMENTS. 125

VIII. REFERENCES. 126

LIST OF FIGURES

Figure		Page
2.1	Light scintillation currents as described by Eq. (2.1) for the BC-444 and BC-418 plastic scintillators	9
2.2	The Schematic Circuit Diagram of a photomultiplier tube.	16
2.3	The calculated voltage pulse from a PMT	20
2.4	The schematic circuit diagram of a delay line with variable attenuation	22
2.5	The schematic circuit diagram of a CR differentiator circuit.	24
2.6	The schematic circuit diagram of a RC integrator circuit.	25
2.7	The schematic circuit diagram of the PMT and single CR differentiator.	28
2.8	Voltage waveforms produced by the circuit diagramed in Fig. 2.7	29
2.9	The schematic circuit diagram of the PMT and double CR differentiation	34
2.10	Voltage waveforms produced by the circuit diagramed in Fig. 2.9	35
2.11	The schematic circuit diagram of the PMT and single RC integrator.	43
2.12	Voltage waveforms produced by the circuit diagramed in Fig. 2.11.	44
2.13	The schematic circuit diagram of the PMT, single CR differentiator, and single RC integrator.	48
2.14	Voltage waveforms produced by the circuit diagramed in Fig. 2.13.	49
3.1	Scintillator light emission spectra	61

Figure		Page
3.2	The light transmittance of each Kodak Wratten Gel filter as a function of wavelength (nm)	65
3.3	RCA 8575 photocathode spectral response characteristics (RCA components 8575 photodetector specification).	67
3.4	Calculated differential PMT charge for two commercial plastic scintillators coupled to a RCA 8575 photomultiplier tube with and without a 1A Wratten Gel optical filter	76
3.5	Schematic diagram of a phoswich detector head for a beta-particle spectrometer	78
4.1	Phoswich detector calculated voltage pulses shaped by a linear spectroscopy amplifier for three different radiation sources: (a) 0.1 MeV normally incident electron, (b) 1.0 MeV normally incident electron, and (c) 1.0 MeV Compton scattered electron absorbed entirely by the thick scintillator.	85
4.2	Schematic circuit diagram of the shaping circuitry of the Ortec Model 460 delay line shaping amplifier connected to the PMT	89
4.3	Phoswich detector calculted voltage pulses shaped by a delay line shaping amplifier for the three different radiation sources: (a) 0.1 MeV normally incident electron, (b) 1.0 MeV normally incident electron, and (c) 1.0 MeV Compton scattered electron absorbed entirely by the thick scintillator.	90
4.4	Phoswich detector calculated voltage pulses shaped by a fast timing filter amplifier for three different radiation sources: (a) 0.1 MeV normally incident electron, (b) 1.0 MeV normally incident electron, and (c) 1.0 MeV Compton electron absorbed entirely by the thick scintillator.	91

Figure		Page
4.5	Gamma ray and beta particle time distribution determined by measuring the zero crossing time of a phoswich detector delay line hspaing amplifier output	93
4.6	Block diagram of the KSU Phoswich beta-particle spectrometer with active gamma ray discrimintion using the zero-crossing time technique.	94
4.7	Time distribution curve of a phoswich detector exposed to $^{137}Cs/^{137m}Ba$ gamma rays and ^{204}Tl beta particles generated using a commercial pulse shape analyzer	96
4.8	Time distribution of mixed filed $^{137}Cs/^{137m}Ba$ and ^{204}Tl radiation measured with a commercial pulse shape analyzer.	97
4.9	Enhanced scale view of the time distribution of $^{137}Cs/^{137m}Ba$ gamma rays and ^{204}Tl beta particles measured with a commercial pulse shape analyzer	98
4.10	Block diagram of the KSU phoswich beta-particle spectrometer with active gamma-ray discrimination using a commercial pulse shape analyzer.	100
4.11	Timing diagram for the zero-crossing-time generated gate input pulse signaling the interaction of a beta particle in the phoswich detector	101
4.12	Timing diagram for the linear gate triggered by beta particle induced gate input signal formation from the phoswich detector and associated electronics	105
5.1	A comparison of the BC-444 scintillator PMT measured and predicted voltage waveforms using the parameters given in Table 5.1	114
5.2	A comparison of the BC-418 scintillator PMT measured and predicted voltage waveforms using the parameters given in Table 5.1	115

Figure		Page
5.3	A comparison of the BC-444 linear spectroscopy amplifier measured and predicted voltage waveforms using the best-fit parameters given in Table 5.1.	117
5.4	A comparison of the BC-418 linear spectroscopy amplifier measured and predicted voltage waveforms using the best-fit parameters given in Table 5.1.	118
5.5	A comparison of the BC-444 delay line shaping amplifier measured and predicted voltage waveforms using the best-fit parameters given in Table 5.1	119
5.6	A comparison of the BC-418 delay line shaping amplifier measured and predicted voltage waveforms using the best-fit parameters given in Table 5.1	120

LIST OF TABLES

Table		Page
3.1	Physical Constants of four plastic scintillators.	62
3.2	The calculated relative total RCA 8575 PMT charge for various combinations of scintillators and Wratten Gel filters for a constant absorbed radiation energy	69
5.1	Laboratory measured best-fit parameters for the scintillators, 1A Wratten Gel filter, RCA 8575 PMT, TENNELEC TC 203BLR linear spectroscopy amplifier, and ORTEC Model 460 delay line shaping amplifier	113

I. INTRODUCTION

Organic (plastic) scintillators have long been used as radiation detectors because of their excellent properties for radiation detection. They are easily fabricated to any shape and size. They can be doped with high atomic number particles to promote gamma ray interactions, or made to have a low atomic number to reduce gamma ray interactions. They can be made with a wide variance in total light output efficiency, characteristic decay time of light phosphorescence, and average wavelength of light emission. They also possess excellent linearity between the total light emission and absorbed radiation energy of gamma rays or beta particles. It is this last property of plastic scintillators which has led to their overwhelming popularity in multi-channel analyzer (MCA) counting systems, where a gamma-ray or beta-particle interaction is recorded in a MCA channel number directly proportional to the amount of absorbed radiation energy. Plastic scintillators are therefore excellent to use to monitor the energy dependence of a radiation field.

However, there are many instances where it is desired to be able to measure the energy composition of a radiation field, and also what fraction of all recorded radiation interactions with a certain energy are beta particles or gamma rays. It is generally very difficult to construct a radiation monitoring system that is sensitive only to beta particles, because beta particles of common energies (0-10 MeV) are stopped within a few centimeters by organic

materials, and gamma rays have a finite probability of interacting with any material. Therefore it is impossible to determine the beta-particle fraction or gamma-ray fraction of all interactions recorded during a single measurement with a single scintillator. A well known passive technique that is used to determine the gamma-ray fraction (and therefore beta-particle fraction) of all radiation interactions is a two measurement, subtraction method. A first measurement is taken with the scintillator exposed to the entire radiation field (gamma + beta). Then, a cover is placed over the scintillator that is thick enough to prevent beta particles from penetrating to the scintillator (gamma only). Then the beta particle energy spectrum can be found by subtracting the gamma only spectrum from the gamma + beta spectrum. However, this method contains a large statistical error, when the statistical error for each measurement is propagated according to statistical error propagation methods. This statistical error for the beta particle spectrum can be greater than the measured beta particle spectrum for relatively low beta-particle count rates in the presence of high gamma-ray flux. Therefore, active methods (methods which identify a radiation interaction as either a gamma ray or a beta particle as the interaction occurs) are desired to reduce the statistical error of a beta field measurement.

One concept of achieving active discrimination between beta particles and gamma rays involves the use of a phoswich detector assembly. A phoswich detector is composed of two or more plastic

scintillators "sandwiched" together. Usually, the top scintillator is very thin and serves as a "sensing" detector for the interaction of beta particles. The bottom thicker scintillator serves as the full radiation energy absorption detector. The physical concept of the use of a phoswich detector is based upon the manner which beta particles and gamma rays interact with the phoswich detector. A beta particle loses energy continuously along its path. Therefore, beta particles normally incident upon the phoswich detector will deposit some energy in the top, thin scintillator. Gamma rays interact mostly by Compton scatter in low atomic number materials, producing an energetic electron that behaves exactly like a beta particle. However, due to the much larger volume of the bottom thick scintillator, most Compton interactions will occur far from the top thin scintillator, and deposit no energy in the top thin scintillator.

There are two basic methods of discriminating between beta particles and gamma rays using the phoswich detector assembly. One method involves viewing the light output from each scintillator separately with two different photo-multiplier tubes (PMT). If an output voltage pulse from the PMT viewing the top thin scintillator is observed, then the radiation interaction is assumed to be a beta particle. Otherwise, the interaction is assumed to be caused by a gamma-ray produced Compton electron. The other method involves viewing the scintillations produced in either scintillator by a single PMT. This is the method studied here. The single PMT views

a composite scintillation light current following radiation interactions with the phoswich detector. If the scintillation decay time constant of the top thin scintillator is much greater than the scintillator decay time constant of the bottom thick scintillator, then a beta-particle interaction will always produce a slowly decaying scintillation light current. Most gamma-ray interactions will produce only a fast decaying scintillation light current. Pulse shape discrimination (PSD) circuitry is then applied to distinguish the presence of the slowly decaying scintillation component. Erkkila (Er85) obtained beta-gamma discrimination by clipping the fast portion of the PMT voltage pulse, and then integrating the remaining PMT voltage pulse. If this integrated value exceeded a certain threshold, then the radiation event was assumed to be a beta particle. Simons (Si85) obtained beta-gamma discrimination by delay line shaping the PMT voltage pulse, and then measuring the time for the voltage pulse to change polarity (zero-crossover). If the zero crossover time occurred after a set time, the radiation event was assumed to be a gamma-ray interaction.

At the time of this publication, there are several design considerations of phoswich detector systems that have not been generally discussed in articles on phoswich beta-gamma spectroscopy. Among these considerations are the optimum thickness of the top thin and bottom thick scintillator, the corresponding maximum possible gamma discrimination ratio, and the inherent distortion of the linearity between the absorbed radiation energy in the phoswich

detector and the assigned MCA channel number. The following report examines phoswich detector assembly design and the theoretical voltage waveforms produced by commerical pulse shape discrimination circuitry, and then compares the theoretical voltage waveforms with laboratory measured voltage waveforms. The results confirm the validity and value of computer modeling for designing a phoswich detector assembly.

II. PHOSWICH DETECTOR PULSE SHAPE ANALYSIS

This section briefly describes the phoswich detector assembly used, explains the expected difference between the current shapes produced by gamma-ray and beta-particle radiation, and then derives the theoretically expected voltage shapes produced by the pulse shape discrimination (PSD) circuits that were examined. The theoretically expected voltage waveforms are derived in detail from an elementary level to benefit a person with a basic understanding of circuit analysis. Many of these equations will be familiar to the experienced instrument designer.

The detector assembly studied in the project consisted of a thin ($\approx$30 mg/cm^2) organic scintillator having a slow ($\approx$180 ns) decay time coupled to a thick (0.5 inch) organic scintillator having a very fast ($\approx$2.5 ns) decay time. Such an assembly "sandwiching" two scintillators is commonly referred to as a phoswich detector. This assembly was chosen so that PSD circuitry could be applied to the voltage pulse produced by a single photomultiplier tube to achieve active pulse-shape discrimination between beta particles and gamma rays. When radiation interacts with an organic scintillator, energy asborbed from the radiation is stored in "trapping levels", and is then dissipated by the release of photons. The rate at which photons are released is determined by the time characteristic of the scintillator. A fast scintillator will release nearly all of the photons within 10 ns after excitation; a slow scintillator will continue to release a significant number of photons after several

hundred nanoseconds. Since a beta particle loses energy continuously along its path, beta particles that are normally incident on the above described phoswich detector will always interact with the top thin scintillator and produce a slowly decaying scintillation current. If the incident beta particle is completely stopped in the thin scintillator, only a slow scintillation current will be produced. If the energy of the incident beta particle is sufficiently large, the beta particle will penetrate to the thick scintillator. In this case, a composite current, consisting of a fast and a slow component, will be produced. But most of the fast component will have decayed away long before the slow component. A gamma ray interacts with the organic detector mostly by Compton scattering, producing an energetic electron. So there is essentially no difference between scintillations produced by gamma rays or beta particles. However, due to the much larger volume of the thick scintillator, gamma radiation is more likely to interact in the thick scintillator than in the thin scintillator. Thus the basis for PSD using a phoswich detector assembly: Beta radiation will <u>always</u> produce a slowly decaying scintillation current; gamma radiation will most likely produce <u>only</u> the fast scintillation current. (Although keep in mind that gamma-ray interactions in the thin scintillator are indistinguishable from beta-particle interactions.)

A. Time Dependent Scintillation Current

Modeling of the voltage pulse shape produced by the PSD circuits is made possible by assuming an empirical fit to the intensity of photons that are emitted after excitation of the scintillator by either gamma-ray or beta-particle interactions. The optical levels in a scintillator can be assumed to both fill and deplete exponentially, so an empirical relation used by Knoll (Kn79) to express the time dependent scintillator current from a single scintillator is:

$$i(t) = I_o(e^{-t/\tau_d} - e^{-t/\tau_r}) \qquad (2.1)$$

where I_o is a measure of the intensity of the light output, τ_d is the decay time constant of the scintillator (ns), and τ_r is the rise time constant of the scintillator (ns). Typical light scintillation currents are shown in Fig. 2.1.

The light emitted by the scintillator varies continuously over wavelengths ranging from about 350 nm to 550 nm. Because the intensity of light output from a scintillator is also dependent on the scintillation efficiency, f (the total number of light photons released per unit of radiation energy absorbed), and the amount of radiative energy absorbed by the scintillator, the intensity of the light output for a single scintillator can be expressed by

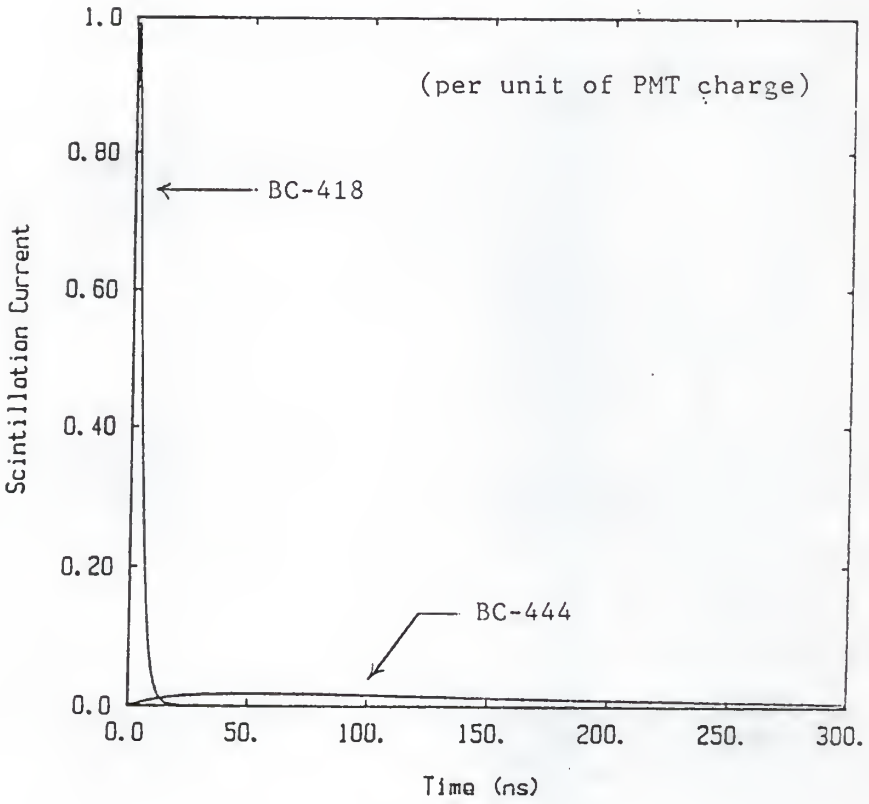

Fig. 2.1 Light scintillation currents as described by Eq. (2.1) for the BC-444 and BC-418 plastic scintillators.

$$I_o = I(E,f,\lambda) = E\ f \int_{\lambda_{min}}^{\lambda_{max}} \epsilon(\lambda)\ d\lambda = E\ f\ , \qquad (2.2)$$

where $\epsilon(\lambda)$ is the normalized photon wavelength distribution function (nm^{-1}) of photons released by the scintillator with wavelength λ. Note that I_o is not a function of time. It determines the magnitude of the scintillation current and is directly proportional to both the amount of radiation energy absorbed in the scintillator and to the scintillation efficiency of the scintillator. It is important to note the wavelength dependence of the light output, because the sensitivity of the photocathode of a PMT is also dependent on photon wavelength. This is discussed in detail in Chapter III, Section III.C.

1. Radiation Energy Absorbed by Each Scintillator

Recall from Eq. (2.2) that the intensity of the light scintillation current can be expressed as a function of the amount of absorbed radiation energy. A model is now needed to predict the amount of radiation energy that will be absorbed by each scintillator of the phoswich detector following interactions with beta particles and gamma rays. It is assumed that beta particles are collimated normally incident on the top thin scintillator, and gamma-ray interactions are equally likely at any point within the volume of the detector. Due to the much larger volume of the thick scintillator, most gamma-ray interactions will occur far from the thin scintillator. Therefore, the Compton electron will deposit all

of its energy in the thick scintillator. The ability of the phoswich detector system to discriminate between gamma-ray interactions and beta-particle interactions is limited physically by the fraction of Compton electrons which deposit a significant amount of energy in the top thin scintillator. Let E_1 be the amount of radiation energy deposited in the top thin scintillator. Let E_2 be the amount of radiation energy deposited in the bottom thick scintillator.

For gamma-ray Compton interactions which occur far from the top thin scintillator, all of the energy of the Compton electron will be deposited in the bottom thick scintillator. Therefore, for gamma-ray Compton interactions

$$E_1 = 0$$

$$E_2 = \text{Compton electron energy.} \tag{2.3}$$

The amount of energy deposited in each scintillator by normally incident beta particles is a bit more complicated to derive. A beta particle loses energy continuously along its path, which scatters randomly throughout the volume of the detector. However, while it is impossible to simply predict the path of an individual beta particle, a statistical penetration length for normally incident beta particles with incident energy E can be calculated using an empirical relation between range and energy (Ch84).

$$R = 0.4\ E^{1.32}\ , \tag{2.4}$$

where R is measured in cm, and E is measured in MeV. Using this relation, the energy E' required for a beta particle to just penetrate the thickness of the thin scintillator is given by

$$E' = (T/0.4)^{1/1.32} , \qquad (2.5)$$

where T is the thickness of the top thin scintillator (cm). Beta particles with energy less than E' will be unable to penetrate to the thick scintillator, and will deposit all of their energy in the top thin scintillator. Therefore for beta particles with incident energy less than E'

$$\left.\begin{aligned} E_1 &= E \\ E_2 &= 0 \end{aligned}\right\} , \quad E \leq E' . \qquad (2.6)$$

Beta particles with incident energy greater than E' will deposit a fraction of their energy in the top thin scintillator and then deposit the remaining energy in the thick scintillator. Using the same relation between beta-particle energy and range

$$\left.\begin{aligned} E_1 &= E - E_2 \\ E_2 &= [(0.4E^{1.32} - T)/0.4]^{1/1.32} \end{aligned}\right\} , \quad E > E' \qquad (2.7)$$

2. Phoswich Detector Scintillation Current

From Section II.A.1, the energy deposited in each scintillator of the phoswich detector by low energy beta particles, high energy

beta particles, and Compton electrons can be calculated. Combining these results with Eqs. (2.1) and (2.2), the scintillation current produced by the phoswich detector can now be written. Let the subscripts 1 and 2 refer to the top thin and bottom thick scintillator, respectively. Then I_1 and I_2 are a measure of the intensity of the light scintillation current produced by the thin and thick scintillators.

A general expression for the light scintillation current produced by the phoswich detector is

$$i(t) = I_1 \left(e^{-t/\tau_{d_1}} - e^{-t/\tau_{r_1}}\right) + I_2 \left(e^{-t/\tau_{d_2}} - e^{-t/\tau_{r_2}}\right) . \qquad (2.8)$$

Now only I_1 and I_2 need to be evaluated for gamma-ray Compton interactions, low energy beta-particle interactions, and high energy beta-particle interactions.

For gamma-ray Compton interactions far from the thin scintillator, no energy is deposited in the thin scintillator. Therefore for Compton interactions

$$I_1 = 0$$

$$I_2 = (\text{energy of Compton electron})\, f_2 . \qquad (2.9)$$

For low energy beta-particle interactions

$$I_1 = E\, f_1$$

$$I_2 = 0 \qquad , \quad E \leq E' \, . \qquad (2.10)$$

For high energy beta-particle interactions

$$I_1 = E_1\, f_1$$

$$I_2 = E_2\, f_2 \qquad , \quad E > E' \, , \qquad (2.11)$$

where E is the energy of the Compton electron or incident beta particle, E' is the energy of a beta particle that will just penetrate the thickness (T) of the thin scintillator and is given by Eq. (2.5), and f is the total light output efficiency of the scintillator. Refer to section II.A.1 for the equations used to determine E_1 and E_2 for high energy beta particles with incident energy greater than E'.

B. Voltage Pulse from the Photomultipler Tube

Now that empirical expressions for the light pulse produced by the scintillator for beta-particle and gamma-ray interactions have been given, the voltage pulse at the anode or a dynode of the photomultiplier tube (PMT) can be examined. Factors affecting the voltage pulse are 1) wavelength dependent sensitivity of the photocathode, 2) gain factor of the PMT, 3) statistical time spread of the electrons arriving and leaving each dynode, and 4) the RC time constant of the dynode or anode of the PMT.

The photons produced during scintillation scatter to the photocathode, where a photoelectric effect occurs, producing electrons which are accelerated to successive dynodes. The number of electrons which are released by the photocathode for each photon absorbed varies with the energy, or wavelength, of the photon. To improve light collection, scintillators are designed to emit most of their light with wavelengths to match the maximum sensitivity of the photocathode, around 400 nm. However, different scintillators will have different light emittance spectra. Thus, the total number of electrons, n_e, leaving the photocathode due to scintillation photons arriving at the photocathode with wavelengths ranging from λ_{min} to λ_{max} is:

$$n_e = E\, f \int_{\lambda_{min}}^{\lambda_{max}} n(\lambda)\, \epsilon(\lambda)\, d\lambda \,, \qquad (2.12)$$

where $n(\lambda)$ is the number of electrons emitted by the photocathode for each incident photon with wavelength λ. These electrons are then accelerated to successive dynodes. At each dynode, the impact of an electron with the surface frees several additional electrons, which are also accelerated to the next dynode, etc. Thus the number of electrons leaving the photocathode is amplified typically by about 10^6 before reaching the anode. Let G be defined as this gain factor. Since not all of the electrons travel to the next dynode with the same path, there is a statistical time spread of the

electrons arriving at the anode. This effect on the pulse shape is negligible for scintillators with long time constants, but must be considered for modeling the pulse shape from fast detectors. However, experimental results show that this statistical time spread does not alter the pulse shape significantly. The RC time constant of the PMT has a much greater effect on the shape of the voltage pulse. A PMT can be simply modeled by the circuit diagram shown in Fig. 2.2.

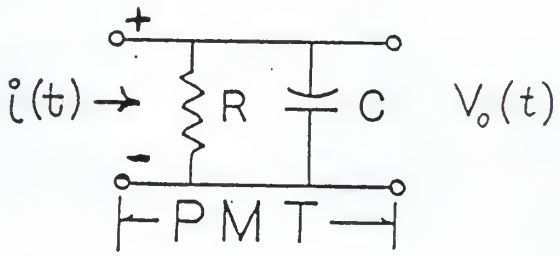

Figure 2.2. The schematic circuit diagram of a photomultiplier tube.

Because the light photons produced by the scintillator interact instantaneously with the photocathode of the PMT, and the electrons released by the photocathode interact instantaneously with successive dynodes of the PMT, the electron current in the PMT has nearly the same time dependence as the light scintillation current. Therefore the electron current in the PMT produced by radiation

interactions in a single scintillator can be expressed similarly to Eq. (2.1),

$$i(t) = I(e^{-t/\tau_d} - e^{-t/\tau_r}) \quad . \tag{2.13}$$

Equation (2.13) is convenient to use to derive an expression for the voltage pulse, $V_{PMT}(t)$, at the PMT anode or n^{th} dynode due to radiation interactions in scintillation detectors. Applying Kirchoff's Current Law to the PMT circuit in Fig. 2.2, it can be shown that

$$i(t) = C \frac{dV_{PMT}(t)}{dt} + \frac{V_{PMT}(t)}{R} \quad , \tag{2.14}$$

where C is the capacitance and R is the equivalent resistance of the PMT. Dividing both sides of Eq. (2.14) by C, and taking the Laplace transform of each side gives the result

$$\frac{\mathcal{L}\{i(t)\}}{C} = [s\mathcal{L}\{V_{PMT}(t)\} - V_{PMT}(0)]$$

$$+ \mathcal{L}\{V_{PMT}(t)\}/RC \quad . \tag{2.15}$$

The required initial condition is that $V_{PMT}(0) = 0$. Thus the overall transfer function of the PMT, defined as the Laplace transform of the output voltage divided by the Laplace transform of the input current is

$$\frac{\mathcal{L}\{V_{PMT}(t)\}}{\mathcal{L}\{i(t)\}} = \frac{1}{C} \frac{1}{s + \frac{1}{RC}} , \qquad (2.16)$$

where s is the Laplace transform variable. The Laplace transform of the scintillation current given by Eq. (2.13), is

$$\mathcal{L}\{i(t)\} = I\left[\frac{1}{s + \frac{1}{\tau_d}} - \frac{1}{s + \frac{1}{\tau_r}}\right] . \qquad (2.17)$$

Therefore, the voltage pulse can be found by taking the inverse Laplace transform of Eq. (2.17).

$$V_{PMT}(t) = \frac{I}{C} \mathcal{L}^{-1} \left\{\frac{1}{s + \frac{1}{RC}} \left[\frac{1}{s + \frac{1}{\tau_d}} - \frac{1}{s + \frac{1}{\tau_r}}\right]\right\} . \qquad (2.18)$$

Thus, the PMT voltage pulse is given by

$$V_{PMT}(t) = \frac{I}{C_{PMT}} \left\{\frac{1}{\frac{1}{\tau_r} - \frac{1}{RC_{PMT}}} e^{-t/\tau_r} - \frac{1}{\frac{1}{\tau_d} - \frac{1}{RC_{PMT}}} e^{-t/\tau_d}\right.$$

$$\left. + \left[\frac{1}{\frac{1}{\tau_d} - \frac{1}{RC_{PMT}}} - \frac{1}{\frac{1}{\tau_r} - \frac{1}{RC_{PMT}}}\right] e^{-t/RC_{PMT}}\right\} . \qquad (2.19)$$

Note that the voltage pulse derived above (Eq. 2.19) is due to scintillations in a <u>single</u> detector. Equation (2.19) can easily be used to predict the voltage pulse created by gamma-ray and beta-particle interactions with the phoswich detector assembly by using

the superposition principle. The voltage pulse due to energy deposited in the slow (thin) scintillator can be found by first calculating I_1 from Section II.A.2 and then substituting I_1 and the slow scintillator parameters into Eq. (2.19). The voltage pulse due to energy deposited in the fast (thick) scintillator can be calculated in a similar manner. Then the total voltage pulse can be found by adding the slow scintillator voltage to the fast scintillator voltage. Figure 2.3 shows PMT voltage pulses.

C. Voltage Pulses from PSD Circuitry

The main purpose of the PSD circuitry is to convert the input voltage pulse (usually from the PMT) into an output waveform whose shape or amplitude varies depending on the type of radiation. Most PSD circuits are designed to detect a difference in one or more of the following four parameters of a voltage pulse: 1) pulse amplitude - either maximum amplitude or amplitude at some fixed time, 2) pulse rise time - the amount of time it takes from when the pulse is first registered to when it reaches some fraction of its peak amplitude, 3) pulse decay time - the amount of time it takes after the pulse registers peak amplitude to when it reaches some fraction of peak amplitude, and 4) pulse zero-crossover time - the amount of time it takes from when the pulse is first registered to when it changes polarity (i.e. crosses the zero voltage-amplitude axis).

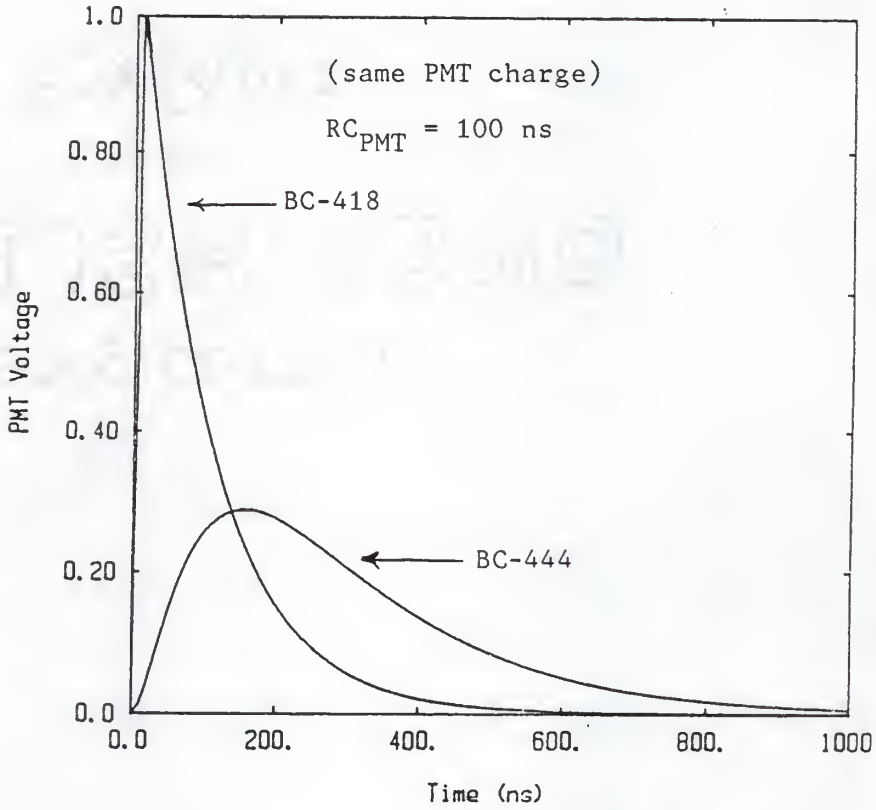

Fig. 2.3. The calculated voltage pulse from a PMT.

The voltage pulse from the PMT usually must be altered in amplitude, length, etc., before being input to analyzing equipment. For example, an MCA requires an input waveform with ~μs decay time, and voltage level between zero and ten volts. Therefore, the voltage pulse from the PMT must be stretched and amplified before being input into the MCA. The most common circuits that do pulse shaping are constructed from some combination of amplifiers, attenuators, CR differentiators, RC integrators, and delay lines. Of course, a look at the electronics inside of a pulse shaping instrument will reveal much more complicated circuitry, such as circuit protectors, and various noise reducing circuitry, but the output waveform of most pulse shaping instruments can be modeled very adequately by the above mentioned circuit components.

1. Delay Line Shaping

Delay lines are very commonly used in pulse-shape discrimination circuitry. For example, a delay line can "hold" a signal while a gate signal is checked. Delay lines are also used to clip a voltage pulse, producing a signal with a specified width. A delay line can be made from a long coaxial cable that is open-circuited at the end. A voltage pulse traveling along this coaxial cable will be reflected back with opposite polarity when it reaches the end of the cable. The typical propagation velocity for a pulse traveling in a coaxial cable is 2/3 of the speed of light. The delay time of a delay line is defined as the time it takes for a

signal to propogate to the end of the delay line, be reflected, and return. Let T_d be the delay time of a delay line. Then from the standard relationship between distance, velocity, and time

$$T_d = 2L/v_p \ . \qquad (2.20)$$

where L is the length of the delay line, and v_p is the propagation velocity of a voltage pulse in the delay line.

When a delay line is connected to a circuit, it passes the arriving signals immediately, then after a delay of T_d, passes a copy of the original signal with reversed polarity. Refer to Fig. 2.4 for a schematic diagram of a delay line.

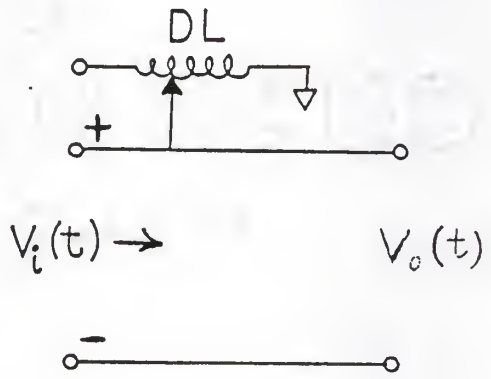

Fig. 2.4. Schematic diagram of a delay line with variable attenuation.

The voltage pulse out of a delay line with delay time T_d is given by

$$V_o(t) = \begin{cases} V_i(t) & , \quad 0 < t < T_d \\ V_i(t) - V_i(t-T_d) & , \quad t > T_d \end{cases} , \qquad (2.21)$$

where $V_o(t)$ is the output voltage pulse, $V_i(t)$ is the input voltage pulse, and T_d is the delay time of the delay line. Some delay line circuitry is designed to provide an attenuated delayed signal. For an example, refer to the Ortec Model 460 Delay Line Amplifier, where an attenuated delayed voltage is used to nearly eliminate the slowly decaying undershoot produced when an exponentially decaying signal is delay-line shaped. For this case,

$$V_o(t) = \begin{cases} V_i(t) & , \quad 0 < t < T_d \\ V_i(t) - f\, V_i(t-T_d) & , \quad t > T_d \end{cases} , \qquad (2.22)$$

where f is the attenuation factor. Note that f = 1 for the case of no attenuation (no reduction in amplitude of delayed signal). Note that Eqs. (2.21) and (2.22) can be used for <u>any</u> input waveform.

2. CR Differentiation and RC Integration

Analysis of the voltage pulse produced by CR differentiation and RC integrators is most easily done by applying a Laplace transform method of solution. To analyze a circuit by a Laplace transform method of solution, simply multiply the overall Laplace

transform of a circuit by the Laplace transform of the input waveform, and then find the inverse Laplace transform of the result. The transfer function for amplifiers and attenuators is simply a constant. Delay lines reflect a delayed copy of the original waveform with reversed polarity. However, differentiators and integrators require a more complex analysis. Fig. 2.5 shows the schematic diagram of a CR differentiator.

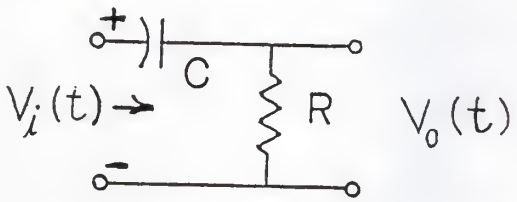

Fig. 2.5. The schematic circuit diagram of of CR differentiator circuit.

Apply Kirchoff's voltage law to the CR differentiator circuit to show that

$$V_i(t) = Q(t)/C + V_o(t) \ , \qquad (2.23)$$

where Q(t) represents the charge stored across the capacitor. Now differentiate each side of Eq. (2.23) with respect to time, so that

$$\frac{d\ V_i(t)}{dt} = \frac{1}{C}\frac{d\ Q(t)}{dt} + \frac{d\ V_o(t)}{dt} \ . \qquad (2.24)$$

Recall dQ(t)/dt = current i(t), so

$$\frac{d\,V_i(t)}{dt} = \frac{i(t)}{C} + \frac{d\,V_o(t)}{dt} \quad . \tag{2.25}$$

Note that $V_o(t) = i(t)\,R$, hence

$$\frac{V_o(t)}{RC} + \frac{d\,V_o(t)}{dt} = \frac{d\,V_i(t)}{dt} \quad . \tag{2.26}$$

Take the Laplace transform of each side of Eq. (2.26), so that

$$\frac{1}{RC}\,\mathcal{L}\{V_i(t)\} + s\mathcal{L}\{V_o(t)\} - V_o(0)$$

$$= s\mathcal{L}\{V_i(t)\} - V_i(0) \quad . \tag{2.27}$$

Assuming initial input and output voltages are zero, the overall transfer function of the CR differentiator is

$$\frac{\mathcal{L}\{V_o(t)\}}{\mathcal{L}\{V_i(t)\}} = \frac{s}{s + \frac{1}{RC}} \tag{2.28}$$

A similar analysis can be applied to the RC integrator. Fig. 2.6 shows the schematic diagram of an RC integrator.

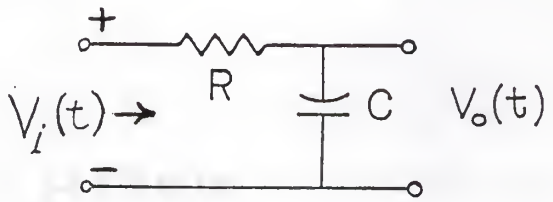

Fig. 2.6. The schematic diagram of an RC integrator circuit.

Apply Kirchoff's voltage law to the RC integrator circuit to show that

$$V_i(t) = i(t)\,R + V_o(t)\ . \tag{2.29}$$

The current and voltage across a capacitor are related by

$$i_c(t) = C\,\frac{d\,V_c(t)}{dt} \tag{2.30}$$

Substitute Eq. (2.30) into Eq. (2.29) to give the result

$$V_i(t) = RC\,\frac{d\,V_o(t)}{dt} + V_o(t)\ . \tag{2.31}$$

Take the Laplace transform of both sides of Eq. (2.31) so that

$$\mathcal{L}\{V_i(t)\} = RC[s\mathcal{L}\{V_o(t)\} - V_o(0)] + \mathcal{L}\{V_o(t)\}\ . \tag{2.32}$$

Thus, assuming initial output voltage is zero, the overall transfer function of the RC integrator is

$$\frac{\mathcal{L}\{V_o(t)\}}{\mathcal{L}\{V_i(t)\}} = \frac{1/RC}{s + 1/RC}\ . \tag{2.33}$$

Now pulse discrimination circuits consisting of CR differentiators, RC integrators, attenuators, and delay lines can be analyzed. The following PSD circuits are all applied to the output of the PMT. To reduce confusion, let RC_{PMT} be the time constant (capacitance multiplied by resistance) of the PMT, and RC_i be the time constant of the i^{th} CR differentiator or RC integrator circuit, accordingly.

Also, let V(t) be the output voltage produced by the following circuits.

3. Single Differentiation of PMT Voltage Pulse

A CR differentiator circuit applied to the PMT output voltage produces a bipolar voltage pulse (single zero-crossover) with a slowly decaying undershoot. This output pulse contains rise time, decay time, and zero-crossover information. Let RC_1 be the time constant of the CR differentiator circuit. Multiply the overall transfer functions of the scintillation current (Eq. 2.17), the photomultiplier tube (Eq. 2.16), and the CR differentiator circuit (Eq. 2.28) to show that the Laplace transfer function for the voltage pulse produced by this system is

$$\mathcal{L}\{V(t)\} = I[(s + 1/\tau_d)^{-1} - (s + 1/\tau_r)^{-1}]$$

$$\cdot \frac{1}{C_{PMT}} \left[s + \frac{1}{RC_{PMT}}\right]^{-1} s \left[s + \frac{1}{RC_1}\right]^{-1} \qquad (2.34)$$

Figure 2.7 shows the schematic circuit diagram, and Fig. 2.8 shows the voltage pulses produced by this circuit. Now find V(t) by taking the inverse Laplace transform of Eq. (2.34).

a. Case One: $RC_{PMT} \neq RC_1$

For this case, apply the distributive property of multiplication to Eq. (2.34) so that

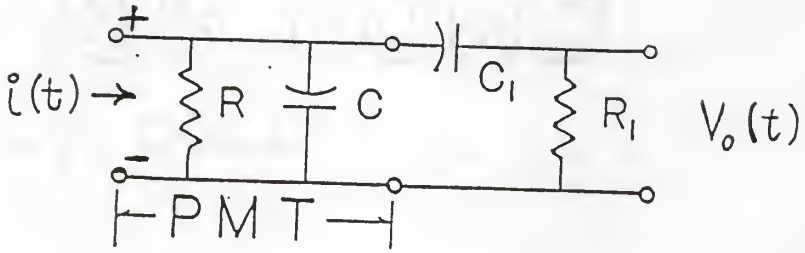

Fig. 2.7. The schematic circuit diagram of the PMT and single CR differentiator.

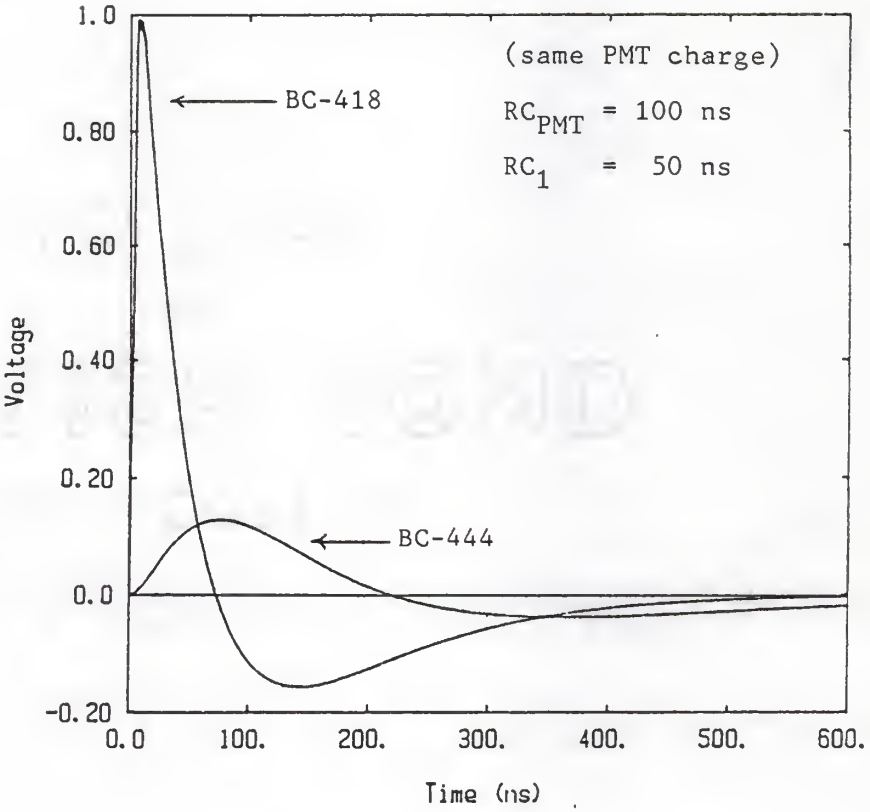

Fig. 2.8. Voltage waveforms produced by the circuit diagrammed in Fig. 2.7.

$$\mathcal{L}\{V(t)\} = \frac{I}{C_{PMT}} \left\{ s \left[(s + 1/\tau_d)\ (s + 1/RC_{PMT})\ (s + 1/RC_1) \right]^{-1} \right.$$

$$\left. - s \left[(s + 1/\tau_r)(s + 1/RC_{PMT})(s + 1/RC_1) \right]^{-1} \right\} . \qquad (2.35)$$

Each [ ] term of Eq. (2.35) has the form

$$f(s) = s[(s+a)(s+b)(s+c)]^{-1} , \qquad (2.36)$$

which has inverse Laplace transform

$$f(t) = a[(a-b)(c-a)]^{-1}\ e^{-at} + b[(b-a)(c-b)]^{-1}\ e^{-bt}$$

$$+ c[(c-a)(b-c)]^{-1}\ e^{-ct} . \qquad (2.37)$$

So, apply the superposition principle to Eq. (2.37) to show that the voltage pulse out of a single CR differentiator with $RC_{PMT} \neq RC_1$ is

$$\frac{C_{PMT}}{I} V(t) = \frac{1}{RC_{PMT}} \left[\frac{1}{RC_{PMT}} - \frac{1}{RC_1} \right]^{-1}$$

$$\cdot \left[\left[\frac{1}{\tau_d} - \frac{1}{RC_{PMT}} \right]^{-1} - \left[\frac{1}{\tau_r} - \frac{1}{RC_{PMT}} \right]^{-1} \right] e^{-t/RC_{PMT}}$$

$$+ \frac{1}{RC_1} \left[\frac{1}{RC_1} - \frac{1}{RC_{PMT}} \right]^{-1} \left[\left[\frac{1}{\tau_d} - \frac{1}{RC_1} \right]^{-1} - \left[\frac{1}{\tau_r} - \frac{1}{RC_1} \right]^{-1} \right] e^{-t/RC_1}$$

$$+ \frac{1}{\tau_d}\left[\left(\frac{1}{\tau_d} - \frac{1}{RC_{PMT}}\right)\left(\frac{1}{RC_1} - \frac{1}{\tau_d}\right)\right]^{-1} e^{-t/\tau_d}$$

$$- \frac{1}{\tau_r}\left[\left(\frac{1}{\tau_r} - \frac{1}{RC_{PMT}}\right)\left(\frac{1}{RC_1} - \frac{1}{\tau_r}\right)\right]^{-1} e^{-t/\tau_r} \qquad (2.38)$$

b. **Case Two:** $RC_{PMT} = RC_1$

Note from Eq. (2.38) that there are discontinuities as RC_{PMT} and CR_1 approach the same value. Let RC_{PMT} and RC_1 = RC in Eq. (2.34). Then the Laplace transfer function of the voltage pulse reduces to

$$\mathcal{L}\{V(t)\} = \frac{I}{C}\left[(s + 1/\tau_d)^{-1} - (s + 1/\tau_r)^{-1}\right]$$

$$\bullet\ s(s + 1/RC)^{-2} \qquad (2.39)$$

As in part a, apply the distributive property of multiplication to Eq. (2.39) to give the result

$$\mathcal{L}\{V(t)\} = \frac{I}{C}\left\{s\left[(s + 1/\tau_d)(s + 1/RC)^2\right]^{-1}\right.$$

$$\left. - s\left[(s + 1/\tau_r)(s + 1/RC)^2\right]^{-1}\right\} \qquad (2.40)$$

Each [ ] term of Eq. (2.40) has the form

$$F(s) = s[(s+a)^2(s+b)]^{-1}\ , \qquad (2.41)$$

which has inverse Laplace transform

$$f(t) = (a-b)^{-2} \left\{ [at(a-b) + b]\, e^{-at} - be^{-bt} \right\} \qquad (2.42)$$

So apply the superposition principle to Eq. (2.42) to show that the voltage pulse out of a single CR differentiator with $RC_{PMT} = RC_1$ is

$$\frac{C_{PMT}}{I} V(t) = \left[\frac{1}{RC} - \frac{1}{\tau_d}\right]^{-2} \left\{ \left[\frac{t}{RC}\left[\frac{1}{RC} - \frac{1}{\tau_d}\right] + \frac{1}{\tau_d}\right] e^{-t/RC} - \frac{1}{\tau_d} e^{-t/\tau_d} \right\}$$

$$- \left[\frac{1}{RC} - \frac{1}{\tau_r}\right]^{-2} \left\{ \left[\frac{t}{RC}\left[\frac{1}{RC} - \frac{1}{\tau_r}\right] + \frac{1}{\tau_r}\right] e^{-t/RC} - \frac{1}{\tau_r} e^{-t/\tau_r} \right\} . \qquad (2.43)$$

4. Double Differentiation of PMT Voltage Pulse

A double CR differentiator circuit applied to the PMT output voltage produces a bipolar voltage pulse similar to the pulse produced by a single CR differentiator, except that the pulse rises faster, and has narrower pulse width. Apply a similar analysis as the single CR differentiator. Let RC_1 and RC_2 be the time constants of the first and second CR differentiator, respectively. Then the Laplace transfer function for the voltage output is

$$\mathcal{L}\{V(t)\} = I\left[\left[s + \frac{1}{\tau_d}\right]^{-1} - \left[s + \frac{1}{\tau_r}\right]^{-1}\right] \frac{1}{C_{PMT}} \left[s + \frac{1}{RC_{PMT}}\right]^{-1}$$

$$\cdot\, s\left[s + \frac{1}{RC_1}\right]^{-1} s\left[s + \frac{1}{RC_2}\right]^{-1} . \qquad (2.44)$$

Figure 2.9 shows the schematic circuit diagram, and Fig. 2.10 shows voltage pulses produced by this circuit. Now find V(t) by taking the inverse Laplace transform of Eq. 2.44.

a. **Case One:** $RC_{PMT} \neq RC_1 \neq RC_2$

Apply the distributive property of multiplication to Eq. (2.44) to show that

$$\mathcal{L}\{V(t)\} = \frac{I}{C_{PMT}} \left\{ s^2 \left[\left[s + \frac{1}{\tau_d} \right] \left[s + \frac{1}{RC_{PMT}} \right] \left[s + \frac{1}{RC_1} \right] \left[s + \frac{1}{RC_2} \right] \right]^{-1} \right.$$

$$\left. - s^2 \left[\left[s + \frac{1}{\tau_r} \right] \left[s + \frac{1}{RC_{PMT}} \right] \left[s + \frac{1}{RC_1} \right] \left[s + \frac{1}{RC_2} \right] \right]^{-1} \right\} . \quad (2.45)$$

Each [ ] term of Eq. (2.45) has the form

$$F(s) = s^2[(s+a)(s+b)(s+c)(s+d)]^{-1} , \quad (2.46)$$

which has inverse Laplace transform

$$f(t) = a^2[(b-a)(c-a)(d-a)]^{-1} e^{-at}$$

$$+ b^2[(a-b)(c-b)(d-b)]^{-1} e^{-bt}$$

$$+ c^2[(a-c)(b-c)(d-c)]^{-1} e^{-ct}$$

$$+ d^2[(a-d)(b-d)(c-d)]^{-1} e^{-dt} . \quad (2.47)$$

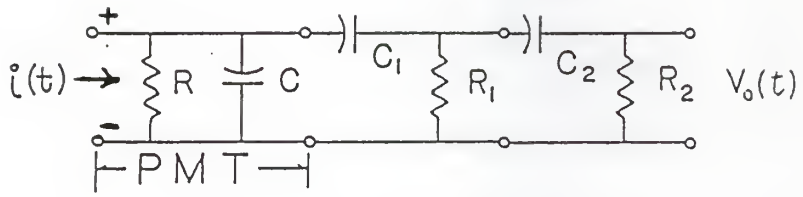

Fig. 2.9. The schematic circuit diagram of the PMT and double CR differentiation.

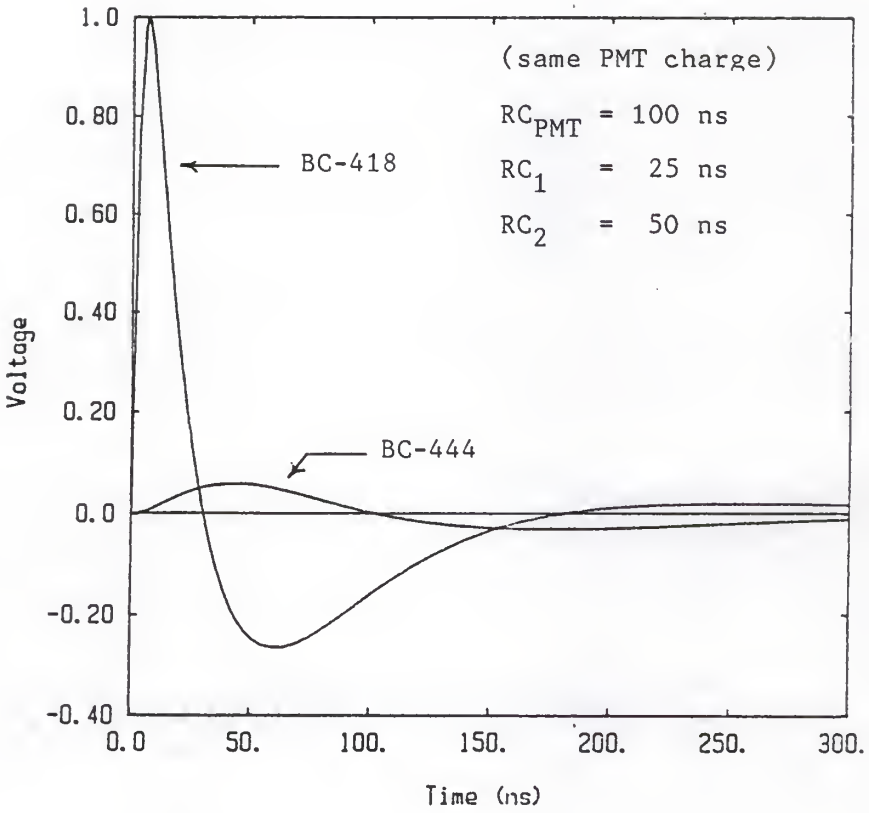

Fig. 2.10. Voltage waveforms produced by the circuit diagrammed in Fig. 2.9.

So apply the superposition principle to Eq. (2.47) to show that the voltage pulse out of a double CR differentiator with $RC_{PMT} \neq RC_1 \neq RC_2$ is

$$\frac{C_{PMT}}{I} V(t) = \left[\frac{1}{RC_{PMT}}\right]^2 \left[\left[\frac{1}{RC_1} - \frac{1}{RC_{PMT}}\right]\left[\frac{1}{RC_2} - \frac{1}{RC_{PMT}}\right]\right]^{-1}$$

$$\cdot \left[\left[\frac{1}{\tau_d} - \frac{1}{RC_{PMT}}\right]^{-1} - \left[\frac{1}{\tau_r} - \frac{1}{RC_{PMT}}\right]^{-1}\right] e^{-t/RC_{PMT}}$$

$$+ \left[\frac{1}{RC_1}\right]^2 \left[\left[\frac{1}{RC_{PMT}} - \frac{1}{RC_1}\right]\left[\frac{1}{RC_2} - \frac{1}{RC_1}\right]\right]^{-1}$$

$$\cdot \left[\left[\frac{1}{\tau_d} - \frac{1}{RC_1}\right]^{-1} - \left[\frac{1}{\tau_r} - \frac{1}{RC_1}\right]^{-1}\right] e^{-t/RC_1}$$

$$+ \left[\frac{1}{RC_2}\right]^2 \left[\left[\frac{1}{RC_{PMT}} - \frac{1}{RC_2}\right]\left[\frac{1}{RC_1} - \frac{1}{RC_2}\right]\right]^{-1}$$

$$\cdot \left[\left[\frac{1}{\tau_d} - \frac{1}{RC_2}\right]^{-1} - \left[\frac{1}{\tau_r} - \frac{1}{RC_2}\right]^{-1}\right] e^{-t/RC_2}$$

$$+ \left[\frac{1}{\tau_d}\right]^2 \left[\left[\frac{1}{RC_{PMT}} - \frac{1}{\tau_d}\right]\left[\frac{1}{RC_1} - \frac{1}{\tau_d}\right]\left[\frac{1}{RC_2} - \frac{1}{\tau_d}\right]\right]^{-1} e^{-t/\tau_d}$$

$$- \left[\frac{1}{\tau_r}\right]^2 \left[\left[\frac{1}{RC_{PMT}} - \frac{1}{\tau_r}\right]\left[\frac{1}{RC_1} - \frac{1}{\tau_r}\right]\left[\frac{1}{RC_2} - \frac{1}{\tau_r}\right]\right]^{-1} e^{-t/\tau_r} . \quad (2.48)$$

Equation (2.48) can be written in a simpler form by letting the subscript 0 replace the subscript PMT, so that $RC_{PMT} = RC_0$. Then Eq. (2.48) reduces to

$$\frac{C_{PMT}}{I} V(t) = \sum_{i=0}^{2} \left[\frac{1}{RC_i}\right]^2 \left[\left[\frac{1}{\tau_d} - \frac{1}{RC_i}\right]^{-1} - \left[\frac{1}{\tau_r} - \frac{1}{RC_i}\right]^{-1}\right] e^{-t/RC_i}$$

$$\cdot \prod_{\substack{j=0 \\ j\neq i}}^{2} \left[\frac{1}{RC_j} - \frac{1}{RC_i}\right]^{-1}$$

$$+ \left[\frac{1}{\tau_d}\right]^2 e^{-t/\tau_d} \prod_{i=0}^{2} \left[\frac{1}{RC_i} - \frac{1}{\tau_d}\right]$$

$$- \left[\frac{1}{\tau_r}\right]^2 e^{-t/\tau_r} \prod_{i=0}^{2} \left[\frac{1}{RC_i} - \frac{1}{\tau_r}\right] . \qquad (2.49)$$

b. Case Two: $RC_{PMT} \neq RC_1 = RC_2$

Note from Eq. (2.43) that there are discontinuities as RC_1 and RC_2 approach the same value. Let RC_1 and $RC_2 = RC_1$ in Eq. (2.44). Then the Laplace transfer function of the voltage pulse reduces to

$$\mathcal{L}\{V(t)\} = \frac{I}{C_{PMT}} s^2 \left[\left[s + \frac{1}{\tau_d}\right]^{-1} - \left[s + \frac{1}{\tau_r}\right]^{-1}\right]$$

$$\cdot \left[s + \frac{1}{RC_{PMT}}\right]^{-1} \left[s + \frac{1}{RC_1}\right]^{-2} \qquad (2.50)$$

Apply the distributive property of multiplication to Eq. (2.50) to give the result

$$\mathcal{L}\{V(t)\} = \frac{I}{C_{PMT}} \left\{ s^2 \left[\left[s + \frac{1}{\tau_d} \right] \left[s + \frac{1}{RC_{PMT}} \right] \left[s + \frac{1}{RC_1} \right]^2 \right]^{-1} \right.$$

$$\left. - s^2 \left[\left[s + \frac{1}{\tau_r} \right] \left[s + \frac{1}{RC_{PMT}} \right] \left[s + \frac{1}{RC_1} \right]^2 \right]^{-1} \right\} . \quad (2.51)$$

Each [ ] term of Eq. (2.51) has the form

$$F(s) = s^2 \, [(s + a)(s + b)^2(s + c)]^{-1} \quad , \quad (2.52)$$

which has inverse Laplace transform:

$$f(t) = a^2[(b-a)^2(c-a)]^{-1} \, e^{-at}$$

$$+ \left\{ b[cb+ab-2ac][(a-b)(c-b)]^{-2} + tb^2[(a-b)(c-b)]^{-1} \right\} e^{-bt}$$

$$+ c^2[(a-c)(b-c)^2]^{-1} \, e^{-ct} \quad . \quad (2.53)$$

So apply the superposition principle to Eq. (2.53) to show that the voltage pulse out of a double CR differentiator with $RC_{PMT} \neq CR_1 = CR_2$ is

$$\frac{C_{PMT}}{I} V(t) = \left[\frac{1}{RC_{PMT}} \right]^2 \left[\frac{1}{RC_1} - \frac{1}{RC_{PMT}} \right]^{-2} \left[\left[\frac{1}{\tau_d} - \frac{1}{RC_{PMT}} \right]^{-1} \right.$$

$$- \left[\frac{1}{\tau_r} - \frac{1}{RC_{PMT}}\right]^{-1}\Bigg] e^{-t/RC_{PMT}}$$

$$+ \left\{\frac{1}{RC_1}\left[(\tau_d\, RC_1)^{-1} + (RC_{PMT}\, RC_1)^{-1} - 2(RC_{PMT}\, \tau_d)^{-1}\right]\right.$$

$$\cdot \left[\left[\frac{1}{RC_{PMT}} - \frac{1}{RC_1}\right]\left[\frac{1}{\tau_d} - \frac{1}{RC_1}\right]\right]^{-2}$$

$$- \frac{1}{RC_1}\left[(\tau_r\, RC_1)^{-1} + (RC_{PMT}\, RC_1)^{-1} - 2(RC_{PMT}\, \tau_r)^{-1}\right]$$

$$\cdot \left[\left[\frac{1}{RC_{PMT}} - \frac{1}{RC_1}\right]\left[\frac{1}{\tau_r} - \frac{1}{RC_1}\right]\right]^{-2}$$

$$\left. + \frac{t}{(RC_1)^2}\left[\frac{1}{RC_{PMT}} - \frac{1}{RC_1}\right]^{-1}\left[\left[\frac{1}{\tau_d} - \frac{1}{RC_1}\right]^{-1} - \left[\frac{1}{\tau_r} - \frac{1}{RC_1}\right]^{-1}\right]\right\} e^{-t/RC_1}$$

$$+ \left[\frac{1}{\tau_d}\right]^2\left[\left[\frac{1}{RC_1} - \frac{1}{\tau_d}\right]^2\left[\frac{1}{RC_{PMT}} - \frac{1}{\tau_d}\right]\right]^{-1} e^{-t/\tau_d}$$

$$+ \left[\frac{1}{\tau_r}\right]^2\left[\left[\frac{1}{RC} - \frac{1}{\tau_r}\right]^2\left[\frac{1}{RC_{PMT}} - \frac{1}{\tau_r}\right]\right]^{-1} e^{-t/\tau_r} . \qquad (2.54)$$

c. Case Three: $RC_{PMT} = RC_1 = RC_2$

Note from Eq. (2.48) that there are discontinuities as RC_{PMT} RC_1 and RC_2 all approach the same value. Let RC_{PMT}, RC_1 and RC_2 all = RC in Eq. (2.44). Then the Laplace transfer function of the voltage pulse reduces to

$$\mathcal{L}\{V(t)\} = \frac{I}{C_{PMT}} s^2 \left[\left[s + \frac{1}{\tau_d} \right]^{-1} - \left[s + \frac{1}{\tau_r} \right]^{-1} \right] \left[s + \frac{1}{RC} \right]^{-3} . \quad (2.55)$$

Apply the distributive property of multiplication to Eq. (2.55) so that

$$\mathcal{L}\{V(t)\} = \frac{I}{C_{PMT}} \left\{ s^2 \left[\left[s + \frac{1}{\tau_d} \right] \left[s + \frac{1}{RC} \right]^3 \right]^{-1} \right.$$

$$\left. - s^2 \left[\left[s + \frac{1}{\tau_r} \right] \left[s + \frac{1}{RC} \right]^3 \right]^{-1} \right\} . \quad (2.56)$$

Each [ ] term of Eq. (2.56) has the form

$$F(s) = s^2 [(s+a)^3 (s+b)]^{-1} , \quad (2.57)$$

which has inverse Laplace transform

$$f(t) = \left[b^2 (b-a)^{-3} - at(2b-a)(b-a)^{-2} + \frac{1}{2} a^2 t^2 (b-a)^{-1} \right] e^{-at}$$

$$- b^2 (b-a)^{-3} e^{-bt} . \quad (2.58)$$

So apply the superposition principle to Eq. (2.58) to show that the voltage pulse out of a double CR differentiator with $RC_{PMT} = RC_1 = RC_2 = RC$ is

$$\frac{C_{PMT}}{I} V(t) = \left\{ \left[\frac{1}{\tau_d}\right]^2 \left[\frac{1}{\tau_d} - \frac{1}{RC}\right]^{-3} - \left[\frac{1}{\tau_r}\right]^2 \left[\frac{1}{\tau_r} - \frac{1}{RC}\right]^{-3} \right.$$

$$- \frac{t}{RC} \left[\left[\frac{2}{\tau_d} - \frac{1}{RC}\right]\left[\frac{1}{\tau_d} - \frac{1}{RC}\right]^{-2} - \left[\frac{2}{\tau_r} - \frac{1}{RC}\right]\left[\frac{1}{\tau_r} - \frac{1}{RC}\right]^{-2} \right]$$

$$\left. + \frac{1}{2} \left[\frac{t}{RC}\right]^2 \left[\left[\frac{1}{\tau_d} - \frac{1}{RC}\right]^{-1} - \left[\frac{1}{\tau_r} - \frac{1}{RC}\right]^{-1} \right] \right\} e^{-t/RC}$$

$$- \left[\frac{1}{\tau_d}\right]^2 \left[\frac{1}{\tau_d} - \frac{1}{RC}\right]^{-3} e^{-t/\tau_d} + \left[\frac{1}{\tau_r}\right]^2 \left[\frac{1}{\tau_r} - \frac{1}{RC}\right]^{-3} e^{-t/\tau_r} \qquad (2.59)$$

5. Single Integration of PMT Voltage Pulse

A single RC integrator circuit applied to the PMT output voltage produces a unipolar voltage pulse. An RC integrator tends to lengthen the pulse, and form a Gaussian shaped output. Let RC_1 be the time constant of the RC integrator circuit. Then the Laplace transfer function of the output voltage produced by the scintillator, PMT, and single RC integrator is

$$\mathcal{L}\{V(t)\} = I[(s + 1/\tau_d)^{-1} - (s + 1/\tau_d)^{-1}]$$

$$\cdot \frac{1}{C_{PMT}} (s + 1/RC_{PMT})^{-1} \frac{1}{RC_1}(s + 1/RC_1)^{-1} . \qquad (2.60)$$

Figure 2.11 shows the circuit diagram, and Fig. 2.12 shows voltage pulses produced by this circuit. Now find V(t) by taking the inverse Laplace transform of Eq. (2.60).

a. **Case One:** $RC_{PMT} \neq RC_1$

For this case, apply the distributive property of multiplication to Eq. (2.60) so that

$$\mathcal{L}\{V(t)\} = \frac{I}{C_{PMT}\, RC_1} \left\{ [(s + 1/\tau_d)(s + 1/RC_{PMT})(s + 1/RC_1)]^{-1} \right.$$

$$\left. - [(s + 1/\tau_r)(s + 1/RC_{PMT})(s + 1/RC_1)]^{-1} \right\} . \qquad (2.61)$$

Each [ ] term of Eq. (2.61) has the form

$$F(s) = [(s+a)(s+b)(s+c)]^{-1} , \qquad (2.62)$$

which has the inverse Laplace transform

$$f(t) = [(b-a)(c-a)]^{-1} e^{-at} + [(a-b)(c-b)]^{-1} e^{-bt}$$

$$+ [(a-c)(b-c)]^{-ct} . \qquad (2.63)$$

So apply the superposition principle to Eq. (2.63) to show that the voltage pulse out of a single RC integrator with $RC_{PMT} \neq RC$ is

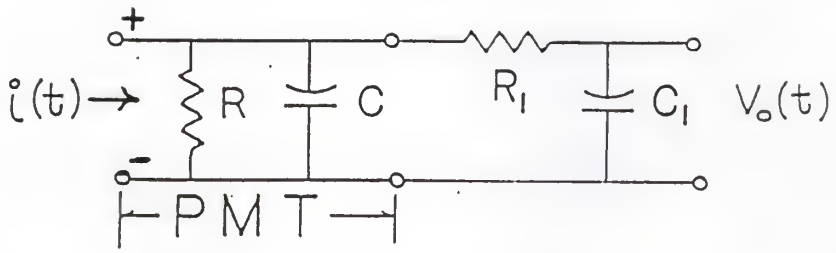

Fig. 2.11. The schematic circuit diagram of the PMT and single RC integrator.

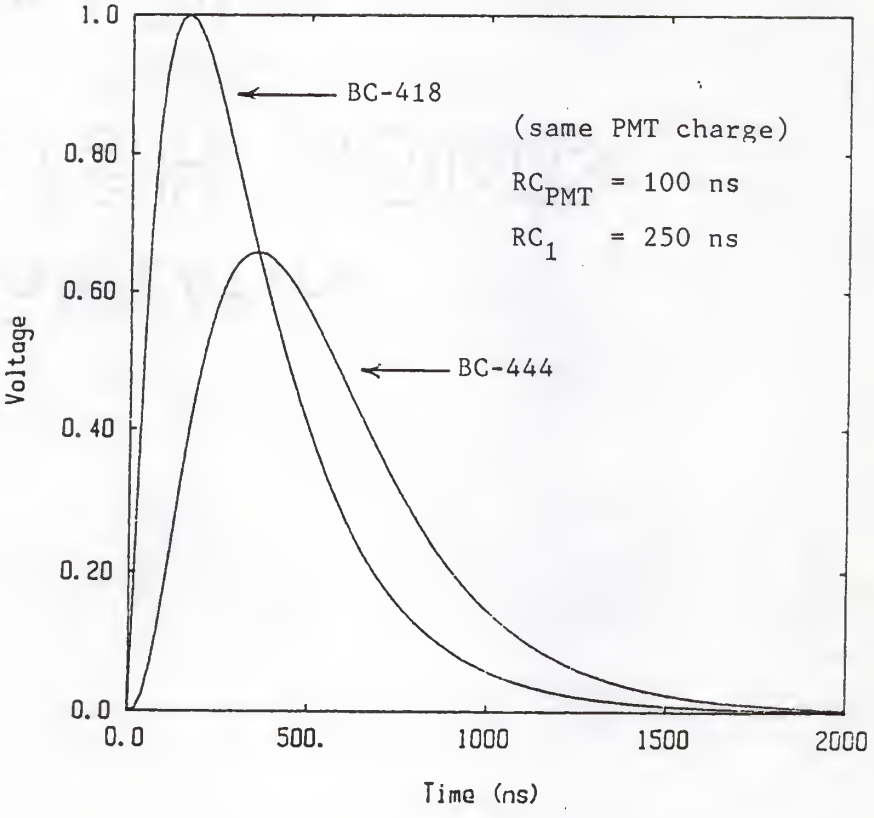

Fig. 2.12. Voltage waveforms produced by the circuit diagrammed in Fig. 2.11.

$$\frac{RC_1\, C_{PMT}}{I} V(t) = \left[\frac{1}{RC_1} - \frac{1}{RC_{PMT}}\right]^{-1}$$

$$\bullet \left[\left[\frac{1}{\tau_d} - \frac{1}{RC_{PMT}}\right]^{-1} - \left[\frac{1}{\tau_r} - \frac{1}{RC_{PMT}}\right]^{-1}\right] e^{-t/RC_{PMT}}$$

$$+ \left[\frac{1}{RC_{PMT}} - \frac{1}{RC_1}\right]^{-1} \left[\left[\frac{1}{\tau_d} - \frac{1}{RC_1}\right]^{-1} - \left[\frac{1}{\tau_r} - \frac{1}{RC_1}\right]^{-1}\right] e^{-t/RC_1}$$

$$+ \left[\left[\frac{1}{RC_{PMT}} - \frac{1}{\tau_d}\right]\left[\frac{1}{RC_1} - \frac{1}{\tau_d}\right]\right]^{-1} e^{-t/\tau_d}$$

$$- \left[\left[\frac{1}{RC_{PMT}} - \frac{1}{\tau_r}\right]\left[\frac{1}{RC_1} - \frac{1}{\tau_r}\right]\right]^{-1} e^{-t/\tau_r} . \qquad (2.64)$$

b. Case Two: $RC_{PMT} = RC_1$

Note from Eq. (2.64) that there are discontinuities as RC_{PMT} and RC_1 approach the same value. Let RC_{PMT} and RC_1 both = RC_1 in Eq. (2.60). Then the Laplace transfer function of the voltage pulse reduces to

$$\mathcal{L}\{V(t)\} = \frac{1}{RC_1\, C_{PMT}} \left[(s + 1/\tau_d)^{-1} - (s + 1/\tau_r)^{-1}\right]$$

$$\bullet (s + 1/RC_1)^{-2} \qquad (2.65)$$

Apply the distributive property of multiplication to Eq. (2.65) so that

$$\mathcal{L}\{V(t)\} = \frac{I}{RC_1 C_{PMT}} \left\{ [(s + 1/\tau_d)(s + 1/RC_1)^2]^{-1} \right.$$

$$\left. - [(s + 1/\tau_r)(s + 1/RC_1)^2]^{-1} \right\}. \qquad (2.66)$$

Each [ ] term of Eq. (2.66) has the form

$$F(s) = [(s+a)(s+b)^2]^{-1} , \qquad (2.67)$$

which has inverse Laplace transform

$$f(t) = (b-a)^{-2} e^{-at} + [t(a-b)^{-1} - (a-b)^{-2}] e^{-bt} . \qquad (2.68)$$

So apply the superposition principle to Eq. (2.68) to show that the voltage pulse out of a single RC integrator with $RC_{PMT} = RC_1$ is

$$\frac{RC_1 C_{PMT}}{I} V(t) = \left[\frac{1}{RC_1} - \frac{1}{\tau_d}\right]^{-2} e^{-t/\tau_d} - \left[\frac{1}{RC_1} - \frac{1}{\tau_r}\right]^{-2} e^{-t/\tau_r}$$

$$+ \left\{ t \left[\left[\frac{1}{\tau_d} - \frac{1}{RC_1}\right]^{-1} - \left[\frac{1}{\tau_r} - \frac{1}{RC_1}\right]^{-1} \right] - \left[\frac{1}{\tau_d} - \frac{1}{RC_1}\right]^{-2} \right.$$

$$\left. + \left[\frac{1}{\tau_r} - \frac{1}{RC_1}\right]^{-2} \right\} e^{-t/RC_1} . \qquad (2.69)$$

6. Differentiation and Integration of PMT Voltage Pulse

A very common shaping amplifier designed to produce a long ($\sim\mu$s) signal to be input into an MCA consists of amplifiers, and a single CR differentiator and single RC integrator. The voltage pulse produced by this circuit is bipolar, with a slowly decaying undershoot. Let RC_1 be the time constant of the differentiator, and RC_2 be the time constant of the integrator. The Laplace transfer function of the voltage output of this system is

$$\mathcal{L}\{V(t)\} = I\,[(s + 1/\tau_d)^{-1} - (s + 1/\tau_d)^{-1}]$$

$$\cdot \frac{1}{C_{PMT}}(s + 1/RC_{PMT})^{-1} s(s + 1/RC_1)^{-1} \frac{1}{RC_2}(s + 1/RC_2)^{-1} \quad . \quad (2.70)$$

Figure 2.13 shows the schematic circuit diagram, and Fig. 2.14 shows voltage pulses from this circuit. Now find V(t) by taking the inverse Laplace transform of Eq. (2.69).

a. Case One: $RC_{PMT} \neq RC_1 \neq RC_2$

For this case, apply the distributive property of multiplication to Eq. (2.70) so that

$$\mathcal{L}\{V(t)\} = \frac{I}{RC_2\, C_{PMT}} \left\{ s[(s + 1/\tau_d)(s + 1/RC_{PMT}) \right.$$

$$\left. \cdot (s + 1/RC_1)(s + 1/RC_2)]^{-1} \right.$$

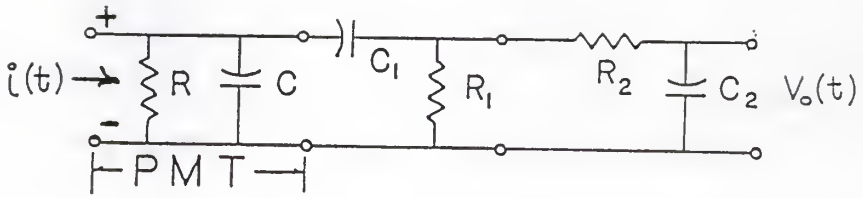

Fig. 2.13. The schematic circuit diagram of the PMT, single CR differentiator, and single RC integrator.

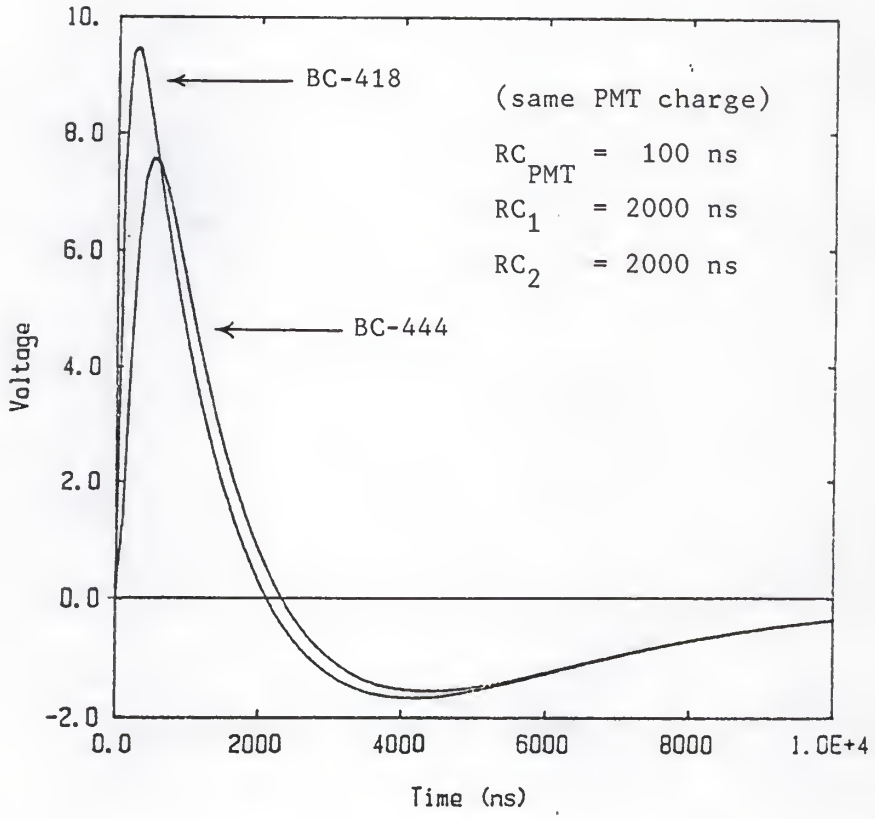

Fig. 2.14. Voltage waveforms produced by the circuit diagrammed in Fig. 2.13.

$$- s[(s + 1/\tau_r)(s + 1/RC_{PMT})(s + 1/RC_1)$$

$$\bullet (s + 1/RC_2)]^{-1}\Big\} \quad . \tag{2.71}$$

Each [ ] term of Eq. (2.71) has the form

$$F(s) = s[(s+a)(s+b)(s+c)(s+d)]^{-1} \quad , \tag{2.72}$$

which has inverse Laplace transform

$$f(t) = a[(a-b)(c-a)(d-a)]^{-1}\, e^{-at} + b[(b-a)(c-b)(d-b)]^{-1}\, e^{-bt}$$

$$+ c[(c-a)(b-c)(d-c)]^{-1}\, e^{-ct} + d[(d-a)(b-d)(c-d)]^{-1}\, e^{-dt} \tag{2.73}$$

So apply the superposition principle to Eq. (2.73) to show that the voltage pulse out of a single CR differentiator and RC integrator with $RC_{PMT} \neq RC_1 \neq RC_2$ is

$$\frac{RC_2\, C_{PMT}}{I} V(t) = \frac{1}{RC_{PMT}} \left[\left[\frac{1}{RC_{PMT}} - \frac{1}{RC_1}\right]\left[\frac{1}{RC_2} - \frac{1}{RC_{PMT}}\right]\right]^{-1}$$

$$\bullet \left[\left[\frac{1}{\tau_d} - \frac{1}{RC_{PMT}}\right]^{-1} - \left[\frac{1}{\tau_r} - \frac{1}{RC_{PMT}}\right]^{-1}\right] e^{-t/RC_{PMT}}$$

$$+ \frac{1}{RC_1}\left[\left[\frac{1}{RC_1} - \frac{1}{RC_{PMT}}\right]\left[\frac{1}{RC_2} - \frac{1}{RC_1}\right]\right]^{-1}$$

$$\cdot \left[\left[\frac{1}{\tau_d} - \frac{1}{RC_1}\right]^{-1} - \left[\frac{1}{\tau_r} - \frac{1}{RC_1}\right]^{-1}\right] e^{-t/RC_1}$$

$$+ \frac{1}{RC_2}\left[\left[\frac{1}{RC_2} - \frac{1}{RC_{PMT}}\right]\left[\frac{1}{RC_1} - \frac{1}{RC_2}\right]\right]^{-1}$$

$$\cdot \left[\left[\frac{1}{\tau_d} - \frac{1}{RC_2}\right]^{-1} - \left[\frac{1}{\tau_r} - \frac{1}{RC_2}\right]\right]^{-1} e^{-t/RC_2}$$

$$+ \frac{1}{\tau_d}\left[\left[\frac{1}{\tau_d} - \frac{1}{RC_{PMT}}\right]\left[\frac{1}{RC_1} - \frac{1}{\tau_d}\right]\right.$$

$$\left.\cdot \left[\frac{1}{RC_2} - \frac{1}{\tau_d}\right]\right]^{-1} e^{-t/\tau_d}$$

$$- \frac{1}{\tau_r}\left[\left[\frac{1}{\tau_r} - \frac{1}{RC_{PMT}}\right]\left[\frac{1}{RC_1} - \frac{1}{\tau_r}\right]\right.$$

$$\left.\cdot \left[\frac{1}{RC_2} - \frac{1}{\tau_r}\right]\right]^{-1} e^{-t/\tau_r} \qquad (2.74)$$

Equation (2.74) can be written in subscript notation by letting $RC_{PMT} = RC_0$. Then Eq. (2.74) reduces to

$$\frac{RC_2\, C_{PMT}}{I} V(t) = \sum_{i=0}^{2} \frac{1}{RC_i}\left[\left[\frac{1}{RC_i} - \frac{1}{\tau_d}\right]^{-1} - \left[\frac{1}{RC_i} - \frac{1}{\tau_r}\right]^{-1}\right] e^{-t/RC_i}$$

$$\cdot \prod_{\substack{j=0 \\ j\neq i}}^{2} \left[\frac{1}{RC_j} - \frac{1}{RC_i}\right]^{-1}$$

$$- \frac{1}{\tau_d} e^{-t/\tau_d} \prod_{i=0}^{2} \left[\frac{1}{RC_i} - \frac{1}{\tau_d}\right]^{-1}$$

$$+ \frac{1}{\tau_d} e^{-t/\tau_d} \prod_{i=0}^{2} \left[\frac{1}{RC_i} - \frac{1}{\tau_r}\right]^{-1} \qquad (2.75)$$

Equation (2.74) can be simplified by examining the actual RC time constants that are commonly used in an actual linear spectroscopy shaping amplifier. Normally, a PMT will be used which has a fast ($\approx$ 100 ns) RC time constant. Differentiation and inntegration time constants will be long (> 1000 ns). Therefore, for RC_1 and $RC_2 >> RC_{PMT}$, and RC_1 and $RC_2 >> \tau_d$ and τ_r, Eq. (2.74) reduces to the approximation

$$\frac{RC_2\, C_{PMT}}{I} V(t) \doteq -RC_{PMT}\left[\left[\frac{1}{\tau_d} - \frac{1}{RC_{PMT}}\right]^{-1} - \left[\frac{1}{\tau_r} - \frac{1}{RC_{PMT}}\right]^{-1}\right] e^{-t/RC_{PMT}}$$

$$- \frac{RC_{PMT}}{RC_1}\left[\frac{1}{RC_2} - \frac{1}{RC_1}\right]^{-1} (\tau_d - \tau_r)\, e^{-t/RC_1}$$

$$- \frac{RC_{PMT}}{RC_2}\left[\frac{1}{RC_1} - \frac{1}{RC_2}\right]^{-1} (\tau_d - \tau_r)\, e^{-t/RC_2}$$

$$+ \tau_d\left[\frac{1}{\tau_d} - \frac{1}{RC_{PMT}}\right]^{-1} e^{-t/\tau_d}$$

$$- \tau_r \left[\frac{1}{\tau_r} - \frac{1}{RC_{PMT}}\right]^{-1} e^{-t/\tau_r} \qquad (2.76)$$

b. Case Two: $RC_{PMT} \neq RC_1 = RC_2$

Note from Eq. (2.74) that there are discontinuties as RC_1 and RC_2 both appproach the same value. Let RC_1 and $RC_2 = RC_1$ in Eq. (2.70). Then the Laplace transfer function of the voltage pulse reduces to

$$\mathcal{L}\{V(t)\} = \frac{I}{RC_1 C_{PMT}} \left[(s + 1/\tau_d)^{-1} - (s + 1/\tau_r)^{-1}\right]$$

$$\bullet\ (s + 1/RC_{PMT})^{-1}\ s(s + 1/RC_1)^{-2} \ . \qquad (2.77)$$

Apply the distributive property of multiplication to Eq. (2.77) so that

$$\mathcal{L}\{V(t)\} = \frac{I}{RC_1 C_{PMT}} \left\{s[(s + 1/\tau_d)(s + 1/RC_{PMT})(s + 1/RC_1)^2]^{-1}\right.$$

$$\left. - s[(s + 1/\tau_r)(s + 1/RC_{PMT})(s + 1/RC_1)^2]^{-1}\right\} . \qquad (2.78)$$

Each [ ] term of Eq. (2.78) has the form

$$F(s) = s[(s+a)(s+b)(s+c)^2] \ , \qquad (2.79)$$

which has inverse Laplace transform

$$f(t) = a[(a-b)(c-a)^2]^{-1}\, e^{-at} + b[(b-a)(c-b)^2]^{-1}\, e^{-bt}$$

$$+ \left\{ ct[(a-c)(c-b)]^{-1} + (ab-c^2)[(b-c)(a-c)]^{-2} \right\} e^{-ct} \qquad (2.80)$$

So apply the superposition principle to Eq. (2.80) to show that the voltage pulse out of a single CR differentiator and RC integrator with $RC_{PMT} \neq RC_1 = RC_2$ is

$$\frac{RC_1\, C_{PMT}}{I} V(t) = \frac{1}{RC_{PMT}} \left[\frac{1}{RC_1} - \frac{1}{RC_{PMT}} \right]^{-2}$$

$$\cdot \left[\left[\frac{1}{RC_{PMT}} - \frac{1}{\tau_d} \right]^{-1} - \left[\frac{1}{RC_{PMT}} - \frac{1}{\tau_r} \right]^{-1} \right] e^{-t/RC_{PMT}}$$

$$+ \left\{ \frac{t}{RC_1} \left[\frac{1}{RC_{PMT}} - \frac{1}{RC_1} \right]^{-1} \left[\left[\frac{1}{RC_1} - \frac{1}{\tau_d} \right]^{-1} - \left[\frac{1}{RC_1} - \frac{1}{\tau_r} \right]^{-1} \right] \right.$$

$$+ \left[(RC_{PMT}\, \tau_d)^{-1} - (1/RC_1)^2 \right] \left[\left[\frac{1}{RC_{PMT}} - \frac{1}{RC_1} \right] \left[\frac{1}{\tau_d} - \frac{1}{RC_1} \right] \right]^{-2}$$

$$\left. - \left[(RC_{PMT}\, \tau_r)^{-1} - (1/RC_1)^2 \right] \right.$$

$$\left. \cdot \left[\left[\frac{1}{RC_{PMT}} - \frac{1}{RC_1} \right] \left[\frac{1}{\tau_r} - \frac{1}{RC_1} \right] \right]^{-2} \right\} e^{-t/RC_1}$$

$$+ \frac{1}{\tau_d}\left[\left[\frac{1}{RC_1} - \frac{1}{\tau_d}\right]^2 \left[\frac{1}{\tau_d} - \frac{1}{RC_{PMT}}\right]\right]^{-1} e^{-t/\tau_d}$$

$$- \frac{1}{\tau_r}\left[\left[\frac{1}{RC_1} - \frac{1}{\tau_r}\right]^2 \left[\frac{1}{\tau_r} - \frac{1}{RC_{PMT}}\right]\right]^{-1} e^{-t/\tau_r} . \quad (2.81)$$

Equation (2.81) can be reduced similarly to Eq. (2.74) for the case where $RC_1 >> RC_{PMT}$ and $RC_1 >> \tau_d$ and τ_r, so that

$$\frac{RC_1 C_{PMT}}{I} V(t) \doteq -RC_{PMT}(\tau_d - \tau_r) e^{-t/RC_{PMT}}$$

$$+ RC_{PMT}(\tau_d - \tau_r)\left[1 - \frac{t}{RC_1}\right] e^{-t/RC_1}$$

$$+ \tau_d \left[\frac{1}{\tau_d} - \frac{1}{RC_{PMT}}\right]^{-1} e^{-t/\tau_d}$$

$$- \tau_r \left[\frac{1}{\tau_r} - \frac{1}{RC_{PMT}}\right]^{-1} e^{-t/\tau_r} \quad (2.82)$$

c. Case Three: $RC_{PMT} = RC_1 = RC_2$

Note from Eq. (2.81) that there are discontinuities as RC_{PMT}, RC_1, and RC_2 all approach the same value. Let RC_{PMT}, RC_1, and RC_2 all = RC in Eq. (2.70). Then the Laplace transfer function of the voltage pulse reduces to

$$\mathcal{L}\{V(t)\} = \frac{I}{C\,RC}\left[(s + 1/\tau_d)^{-1}\right.$$

$$\left. - (s + 1/\tau_r)^{-1}\right] s\,(s + 1/RC)^{-3} \qquad (2.83)$$

Apply the distributive property of multiplication to Eq. (2.83) so that

$$\mathcal{L}\{V(t)\} = \frac{I}{C\,RC}\left\{s[(s + 1/\tau_d)(s + 1/RC)^3]^{-1}\right.$$

$$\left. - s[(s + 1/\tau_r)(s + 1/RC)^3]^{-1}\right\} . \qquad (2.84)$$

Each [ ] term of Eq. (2.84) has the form

$$F(s) = s[(s+a)^3(s+b)]^{-1} , \qquad (2.85)$$

which has inverse Laplace transform

$$f(t) = \left[\frac{1}{2}\,at^2(a-b)^{-1} + bt(b-a)^{-2} + b(a-b)^{-3}\right] e^{-at}$$

$$+ b(b-a)^{-3}\, e^{-bt} . \qquad (2.86)$$

Apply the superposition principle to Eq. (2.86) to show that the voltage pulse out of a single CR differentiator and RC integrator with $RC_{PMT} = RC_1 = RC_2$ is

$$\frac{C\,RC}{I}\,V(t) = \left\{\frac{t^2}{2\,RC}\left[\left[\frac{1}{RC} - \frac{1}{\tau_d}\right]^{-1} - \left[\frac{1}{RC} - \frac{1}{\tau_r}\right]^{-1}\right]\right.$$

$$+ t \left[\frac{1}{\tau_d} \left(\frac{1}{\tau_d} - \frac{1}{RC} \right)^{-2} - \frac{1}{\tau_r} \left(\frac{1}{\tau_r} - \frac{1}{RC} \right)^{-2} \right]$$

$$+ \frac{1}{\tau_d} \left(\frac{1}{\tau_d} - \frac{1}{RC} \right)^{-3} - \frac{1}{\tau_r} \left(\frac{1}{\tau_r} - \frac{1}{RC} \right)^{-3} \Bigg\} e^{-t/RC}$$

$$- \frac{1}{\tau_d} \left(\frac{1}{\tau_d} - \frac{1}{RC} \right)^{-3} e^{-t/\tau_d} + \frac{1}{\tau_r} \left(\frac{1}{\tau_r} - \frac{1}{RC} \right)^{-3} e^{-t/\tau_r} \quad . \quad (2.87)$$

III. PHOSWICH DETECTOR ASSEMBLY

Each detector assembly consisted of some combination of encapsulated plastic scintillators with and without an optical filter (the detector head), a PMT (photomultiplier tube), a magnetic shield, and a PMT voltage divider having both an anode and dynode output. Many combinations of scintillators were tested. Two PMT's were evaluated, an RCA 8575 and an RCA 8850. Voltage divider strings designed for fast pulse applications allowed meaningful gamma-ray discrimination. The gamma-ray discrimination section of the associated electronics was connected to the detector assembly starting at the 50 ohm anode. This anode signal was passed through a short piece of matched 50 ohm coaxial cable to the 50 ohm pre-amplifier input. For the linear signal, the dynode output was connected to a standard type scintillation preamplifier designed for slow linear tail pulses. Information on phoswich detector design and construction applied to beta-particle spectrum measurements using plastic scintillators is examined in this section.

A. Plastic Scintillators

Plastic scintillators are very well suited for detecting beta particles as well as for the total absorption detector in a beta-particle spectrometer. Upon combining these two applications into a single detector head one obtains the subject detector--the plastic phoswich detector with active gamma-ray discrimination. Plastic

scintillators exhibit excellent linearity between light output and absorbed radiation energy and they have a desirable low atomic number. Operating a detector with a low atomic number provides the potential of obtaining tissue equivalent dose information and it ensures a minimum probability of gamma ray interaction. Conversely, however, when gamma rays do interact in a plastic scintillator, Compton electrons, particles which are identical to beta particles and have a continuous energy distribution, are produced. As these charged particles (electrons or beta particles) pass through the plastic detector they lose energy continuously along their path. A fraction of this energy goes into molecular excitation which in turn leads to photon emission. However, when a single plastic scintillation detector is used, it is impossible to distinguish between pulses formed by interactions which stem from gamma-ray interference and those derived directly from beta particle energy deposition.

It is possible to distinguish between interactions which occur in different types of plastic scintillation detectors because the luminescence of a plastic scintillator is time dependent as well as electron energy dependent. This is the basic principle behind the operation of a phoswich detector. The time dependence of the light emitted by a single scintillator, following excitation by either a beta particle or a gamma ray, is given by the expression,

$$i(t) = I_o(E,f,\lambda)\ (e^{-t/\tau_d} - e^{-t/\tau_r}). \qquad (3.1)$$

where $I_o\ (E,f,\lambda)$ is a measure of the total rate at which photons are

released by the scintillator following excitation, E is the amount of absorbed energy, f is the light output efficiency of the scintillator, λ is the wavelength of the photons released during the scintillation process, τ_d is the decay time constant of the scintillator and τ_r is the rise time constant of the scintillator.

Furthermore, (as shown in Fig. 3.1) the photon emission spectra are detector-type dependent. Normally, for a single detector it is desirable to match the spectral response of the PMT to the emission spectrum. This wavelength dependence is important to recall because the sensitivity of the photomultiplier tube's photocathode is also wavelength dependent. Interestingly enough, this property adds an important additional design parameter which not only can but must be considered when two or more plastic scintillators are placed together.

In designing the phoswich detector assemblies, decay time and spectral emission were both considered. On this basis, three total energy absorption plastics with fast decay times were chosen for evaluation--BC-400, BC-418 and BC-422. The beta-particle sensor was a BC-444 detector with a long decay time. These were factory machined and polished cylindrical detectors with diameters of 50.8 mm (2 in.) and various thicknesses. Some characteristics of these detectors, purchased from the Bicron Corp., 12345 Kinsman Road, Newbury, Ohio 44065, are given in Table 3.1.

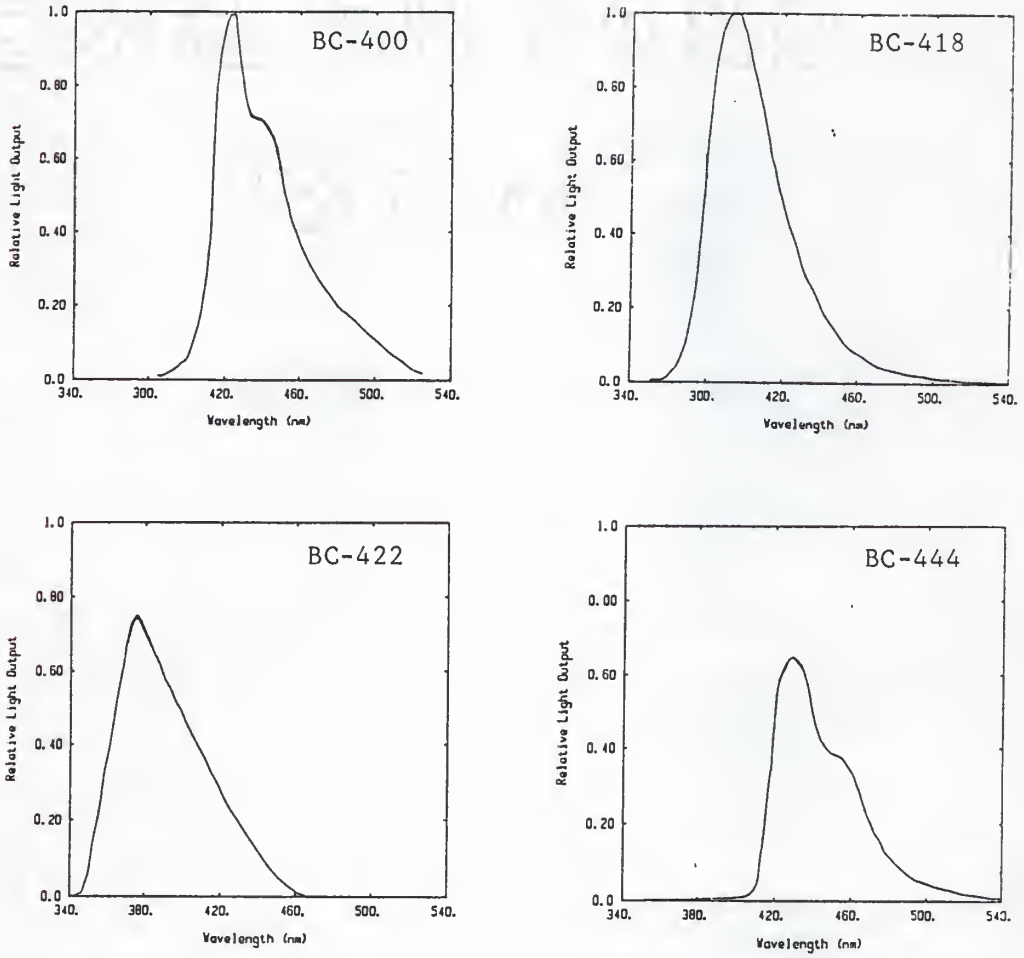

Fig. 3.1. Scintillator light emmission spectra.
(Reproduced from manufacturer specifications).

Table 3.1. Physical constants of four plastic scintillators.[a]

Scintillator	Density	Refractive Index	Light Output (% anthracene)	Rise Time Constant (ns)	Decay Time Constant (ns)	FWHM (ns)	Wavelength of Max. Emission (nm)
BC-400	1.032	1.581	65	0.9	2.4	2.7	423
BC418	1.032	1.58	67	0.5	1.4	1.2	391
BC-422	1.032	1.58	55	0.35	1.6	1.3	370
BC-444	1.032	1.58	41	19.5	179.7	171.9	428

[a]Data obtained from the manufacturer

B. Wratten Gel Optical Filters

To pursue photon emission spectral design considerations, the transmission specifications for several different Kodak Wratten Gel filters were used to predict the change in PMT sensitivity when one of these filters was inserted between the phoswich detector and the photocathode. By examining the differences in the relative light output spectra of the four plastic scintillators shown in Fig. 3.1 and the light output values listed in Table 3.1, it is apparent that there are significant differences in the wavelength dependent light emission of each scintillator. Furthermore, as discussed in detail in Section III.C, the photoelectric conversion at the photocathode of a PMT is dependent upon the wavelength of the incident light. This could result in a nonlinear relationship between PMT output charge and deposited beta particle energy when the light emission from a phoswich (two detectors) is added together. More detailed energy nonlinearity information is presented in Section III.D.3. Experimental results (see Chapter 5) validated the usefulness of these filters.

Because of their convenient form, several Wratten Gel filters were selected. Their effects were examined as a means of eliminating distortions in the measured beta-particle pulse height distribution and to determine if the gamma-ray discrimination properties could be improved. These filters are produced by their manufacturer by dissolving a variety of organic dyes in a liquid gelatin solution. The dried film is coated with lacquer to form a

0.1 mm thick filter. Wratten Gel filters have a melting point of 50 C and are hygroscopic. Care was taken to protect them from high temperatures and humidity during storage. Once they were sealed inside the detector assembly, they did not require special consideration. Selection of this type of filter allowed us to obtain an inexpensive set of filters that had appropriate transmission properties that could easily be cut to fit between the detector and the PMT. Typical absorption curves of several potentially useful Kodak Wratten Gel filters are shown in Fig. 3.2.

C. Photomultiplier Tube Characteristics

The overall response of any scintillation-based radiation detector depends upon the spectral match between the detector and the PMT. This is doubly important when two scintillators are placed together and viewed by a single PMT.

1. PMT Electron Current Pulse

When a single detector or a phoswich detector is placed in a beta or gamma radiation field, electrons slowing down within the scintillator(s) will produce photons that scatter to the photocathode of the single PMT. For a phoswich, photons emitted by the individual scintillators will sum to produce a composite result. The number of photoelectrons released at the photocathode varies with the wavelengths of the composite photon field. Spectral matching is normally used to optimize the number of photoelectrons

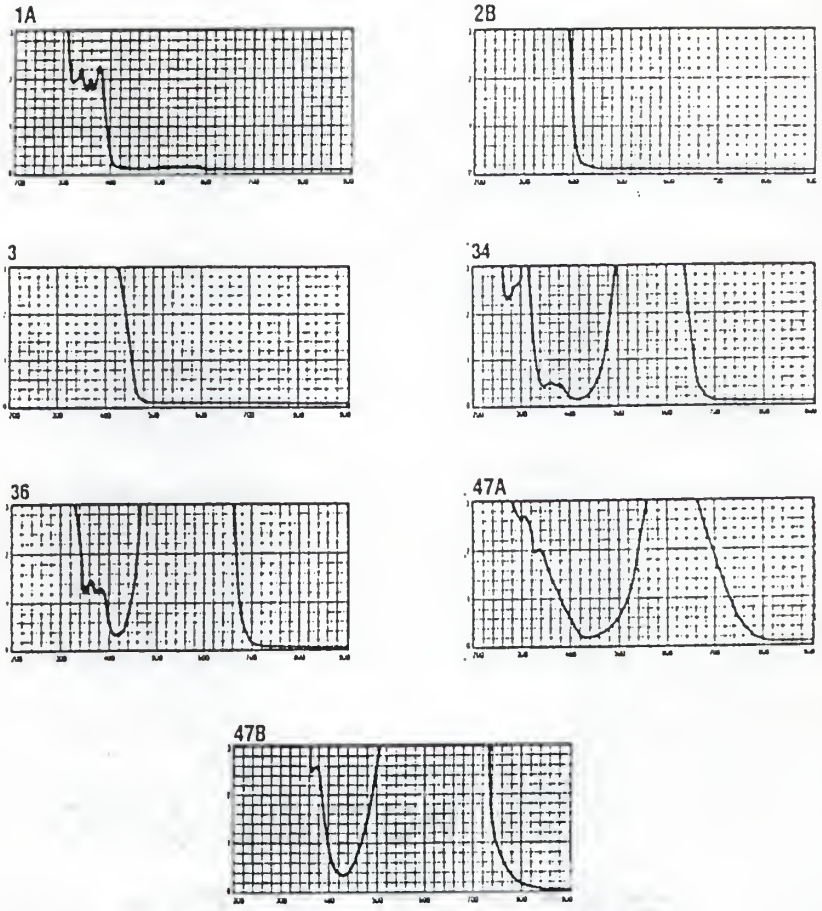

Fig. 3.2. The light transmittance of each Kodak Wratten Gel optical filter as a function of wavelength (nm). Scale is negative log of the fractional transmittance. (Obtained from manufacturer specifications).

released at the photocathode and reduce the statistical spread in the final number of electrons arriving at the anode. This in turn improves the resolution of the spectrometer. Many scintillation detectors are designed to be used with PMTs having photon wavelength dependent sensitivities similar to those shown in Fig. 3.3 for the RCA 8575 PMT used in this study. Lastly, the very small electron current released at the photocathode is amplified by passage through the dynode chain. As a result of electrons following slightly different paths between dynodes, there will be some time dispersion at the last dynode and anode. For most practical cases this time spread will have a very small effect of the time distribution of the pulse formed by interactions occurring within the scintillator.

2. Relative PMT Charge

The electron charge produced in the PMT is equal to the integrated current and can be made directly proportional to the amplitude of the voltage pulse processed to obtain the desired pulse height distribution. It is therefore desirable to examine the factors influencing the charge produced in the PMT. For a given combination of a single scintillator, Wratten Gel filter, and PMT, the total charge produced in the PMT, defined as the total number of electrons collected at the anode of the PMT, is given by

$$Q = E\ f\ G \int_{\lambda_{min}}^{\lambda_{max}} \epsilon(\lambda)T(\lambda)n(\lambda)d\lambda \qquad (3.2)$$

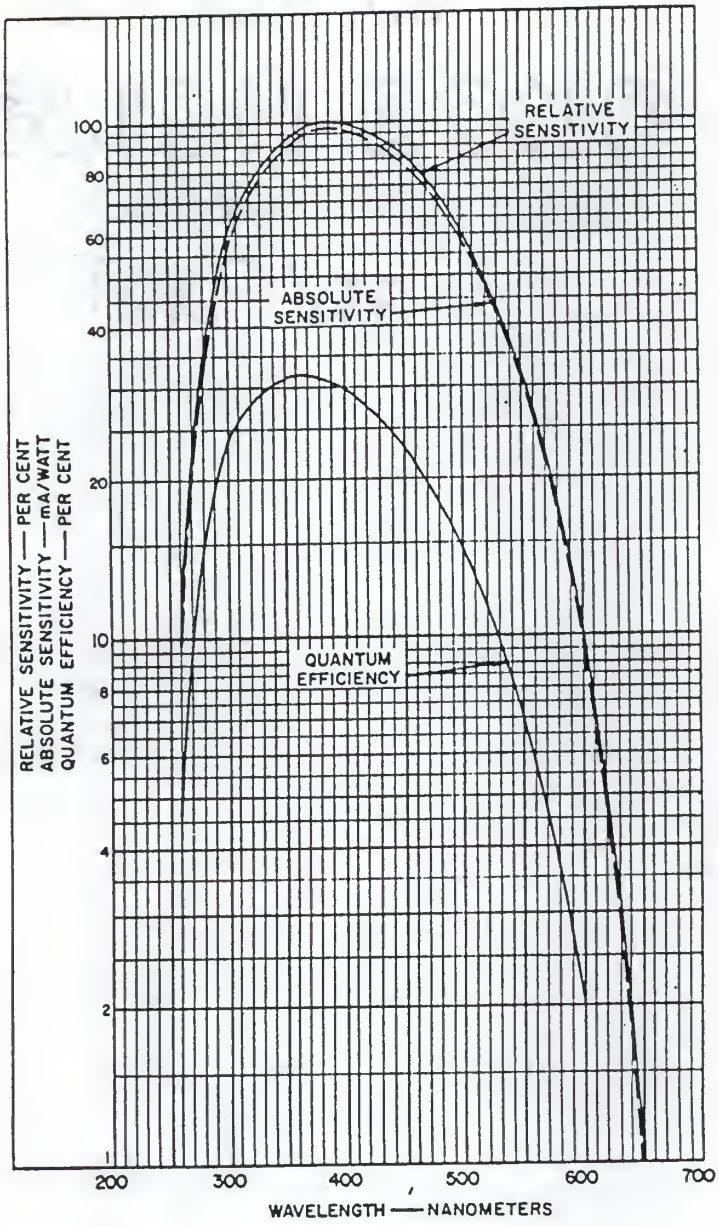

Fig. 3.3. RCA 8575 photocathode spectral response characteristics. (RCA Components 8575 Photodetector specification).

where E is the amount of absorbed radiation energy, f is the scintillator output efficiency, G is the gain factor of the PMT, λ_{min} is the minimum and λ_{max} is the maximum wavelength of the emission spectrum of the scintillator, $\epsilon(\lambda)$ is the normalized wavelength distribution function of photons emitted by the scintillator with wavelength λ, $T(\lambda)$ is the fractional transmittance of the Wratten Gel filter for photons having a wavelength of λ (1.0 for no filter), and $n(\lambda)$ is the number of electrons emitted by the photocathode for each photon absorbed with wavelength λ. Equation (3.2) was used to calculate the charge for various combinations of scintillators, filters, and PMTs. The normalized results are shown in Table 3.2. Note that for the same amount of absorbed energy, the total PMT charge can differ by several orders of magnitude.

D. Detector Assembly Overall Sensitivity

The detector assembly, consisting of the phoswich detector, the PMT, and the voltage divider string (VDS), produces a single voltage pulse per interaction which contains information identifying both radiation type and energy. Analyzing equipment can extract only the information contained in this voltage pulse. Therefore, for phoswich detector design, it is useful to identify the factors affecting pulse formation and hence, the potential to both discriminate between types of radiation and measure beta-particle energy.

Table 3.2. The relative total RCA 8575 PMT charge for various combinations of scintillators and Wratten Gel filters for a constant absorbed radiation energy.

Scintillator	Wratten-Gel Filter	Relative Total PMT Charge[a]
BC-400	None	87.9
	1A	66.3
	2B	60.1
	3	11.7
	34	43.4
	36	22.1
	47A	49.5
	47B	27.8
BC-418	None	100
	1A	40.3
	2B	25.3
	3	2.1
	34	55.1
	36	22.9
	47A	33.8
	47B	17.8
BC-422	None	82.7
	1A	21.0
	2B	12.6
	3	0.2
	34	40.1
	36	14.0
	47A	20.0
	47B	9.8
BC-444	None	54.9
	1A	42.0
	2B	39.4
	3	7.7
	34	25.7
	36	12.3
	47A	32.0
	47B	17.5

[a]Relative to the BC-418 scintillator.

1. Maximum Gamma-Ray Discrimination Ratio

The ability to discriminate between beta-particle and gamma-ray interactions is based on the manner in which the two types of radiation interact with plastic scintillators. Beta particles lose energy continuously along their path. Gamma rays interact at discreet points in the scintillator, mostly by Compton scattering, producing an energetic electron which behaves exactly like a beta particle with the same energy. Thus a beta particle normally incident upon the phoswich detector will deposit energy in both the top thin scintillator and the bottom thick scintillator. If the top thin scintillator has a very slow decay time constant, and the bottom thick scintillator has a very short decay time constant, then a beta particle will always produce a light scintillation current with a slowly decaying component. A statistical penetration length through a scintillator can be calculated for normally incident beta particles. Using this relationship between beta particle energy and penetration length, the amount of energy required for a beta particle to penetrate through the thin scintillator can be calculated. Let this energy be E'. Then beta particles with incident energy less than E' will produce only a slow scintillation current. Beta particles with incident energy greater than E' will lose some of their energy in the thin scintillator, and deposit their remaining energy in the thick scintillator. Thus the light scintillation current produced by high energy beta particles will consist of both a rapidly decaying pulse and a slowly decaying

pulse. Gamma rays can interact with either the thin scintillator or the thick scintillator. Gamma ray interactions in the thin scintillator will deposit energy in the thin scintillator, producing a slow light scintillation current that is indistinguishable from a beta particle interaction. Gamma rays that interact in the thick scintillator near the thin scintillator create an electron which may scatter into the thin scintillator, producing both slow and fast decaying light scintillation com-ponents. Gamma rays that interact in the thick scintillator, but well-separated from the thin scintillator will create an electron that is entirely stopped in the thick scintillator, producing only a fast decaying light scintillation component.

The gamma discrimination ratio can be defined as the total number of gamma-ray interactions in the detector for each gamma-ray interaction that is not identified. It is evident that the maximum possible gamma discrimination ratio is the ratio of the probability of a gamma-ray interaction with either scintillator to the probability of a gamma-ray interaction with the thin scintillator. This ratio is easily approximated by noting the very small mass interaction coefficient for gamma rays in plastic scintillators. Then, for a homogeneous angular distribution of gamma-ray flux, the gamma discrimination ratio can be estimated by the ratio of the thickness of the thick and thin detector

$$\text{Gamma-Ray Discrimination Ratio} = (D_{thick} + D_{thin})/D_{thin} \, , \qquad (3.3)$$

where D_{thick} is the thickness of the thick scintillator, and D_{thin}

is the thickness of the thin scintillator. However, consider a Compton recoil electron created in the thick scintillator that scatters into the thin scintillator and deposits a significant amount of energy in the thin scintillator. Assuming an average typical Compton electron energy of 500 keV (penetration range = 1.6 mm), it is clear that a significant fraction of gamma-ray interactions occurring within 1.6 mm from the thin scintillator will deposit energy in the thin scintillator, and thus be mistaken for beta particles. In fact, for small thicknesses of the thin scintillator (< 0.3 mm), and a homogeneous angular distribution of gamma-ray flux, more Compton electrons created in the thick scintillator may scatter to the thin scintillator than the number of electrons created in the thin scintillator itself. So when one considers these effects as well as afterglow in the fast scintillator the actual gamma discrimination ratio is certainly less than predicted by Eq. (3.3).

2. Optimum Total Thickness of the Phoswich Detector

From Eq. (3.3), it is easily seen that the maximum gamma discrimination ratio can be improved by either making the thin scintillator thinner, or by making the thick scintillator thicker. As the thin scintillator is made thinner and thinner, the amplitude of the slow light scintillation current becomes smaller and smaller. Eventually the amplitude is too small to be detected by the analyzing circuitry so there is a lower limit to how thin the thin

scintillator can be. The maximum thickness of the thick scintillator is limited theoretically by the light absorption of the thick scintillator to both its own wavelengths, and the wavelengths of the thin scintillator light current. However, before the light absorption has any significant effect on the light scintillation current reaching the photocathode of the PMT, a practical consideration presents a realistic limit to the thickness of the thick scintillator. A 12.7 mm thick plastic scintillator will stop a 2.7 MeV beta particle. So the use of thicker scintillators will not improve the ability of a detection system to measure the energy of normally incident beta particles with energies less than 2.7 MeV. A thicker scintillator will only enhance the total number of gamma-ray interactions. In other words, the sensitivity of the detector to normally incident beta particles is dependent on the surface area of the detector, while the sensitivity of the detector to gamma rays is dependent on both the surface area and the thickness of the detector. Thus the optimum total thickness of the phoswich detector is that thickness that will just stop the highest energy normally incident beta particles that are to be measured. The optimum thickness of the thin scintillator is a compromise between the desire to have a low probability of Compton interactions with the thin scintillator, and the minimum required amplitude of the slow scintillation current as compared to the fast scintillation current produced by high energy beta particles.

3. Energy Nonlinearity

The thick and thin scintillators differ in their decay time constants, emission spectra, and relative light output. Previous sections have discussed the desirability of these differences for the design of a phoswich detector to be used in a beta spectrometer system. However, these differences can result in an undesired distortion in the energy vs. channel number for the beta-particle spectrum recorded by a phoswich detector counting system.

A detector system using a single scintillator to monitor the radiation field provides an output signal whose amplitude varies linearly depending on the amount of absorbed radiation energy. Shaping circuits applied to the output signal of a PMT are designed to preserve this linearity between pulse amplitude and absorbed radiation energy.

However, detection systems using a phoswich detector do not have this inherent linear relationship between absorbed radiation energy and pulse amplitude. Factors which distort the linearity of the phoswich detector system are total light emission, the difference in scintillator light emission spectra and the difference in the rise time constants and decay time constants of the two scintillators.

The total light reaching the PMT photocathode can be changed by placing an optical filter between the detector and the PMT. Since the thick and thin scintillators can be selected so that the light

emission spectrum of one is shifted from the other, it is conceivably possible to insert a Wratten-Gel filter to selectively adjust the relative amount of light that reaches the photocathode of the PMT produced by the thick and thin scintillator so that a given amount of radiation energy absorbed in either scintillator will produce the same total PMT charge. An example of how filters can be used to "fine tune" a phoswich detector system is shown in Fig. 3.4. For research purposes, this technique is easier and more versatile than trying to fabricate scintillators with a specified light output.

E. Construction of KSU Phoswich Detector Assemblies

During assembly of the detector head (see Fig. 3.5), a total energy absorption detector was coupled to a 50.8 mm diameter PMT using Bicron optical coupling grease. If a plastic beta-sensor detector was used, it was placed on top (no coupling grease) of the thicker detector. There were two reasons for not using coupling grease between the plastic detectors. The grease attenuated the incident beta particles before they entered the total energy absorption detector and it made changing thin detectors more difficult. If a Wratten Gel filter was used, it was optically coupled to the PMT and then the thicker plastic detector was optically coupled to the filter. They were then fitted with a light-tight 0.96 mg/cm thick aluminized Mylar window. The side surface of the detector was also covered with reflective aluminized Mylar. A black plastic sleeve was then slipped over the detector

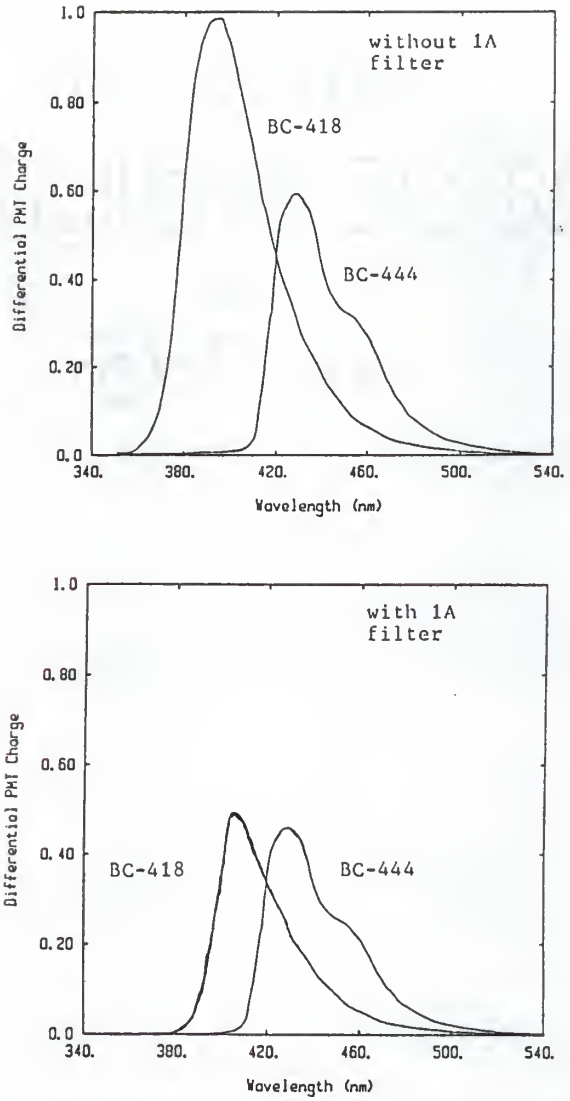

Fig. 3.4. Calculated differential PMT charge for two commercial plastic scintillators coupled to a RCA 8575 photomultiplier tube with and without a 1A Wratten Gel optical filter.

and attached with black tape. These procedures were designed for ease of changing the detector combinations.

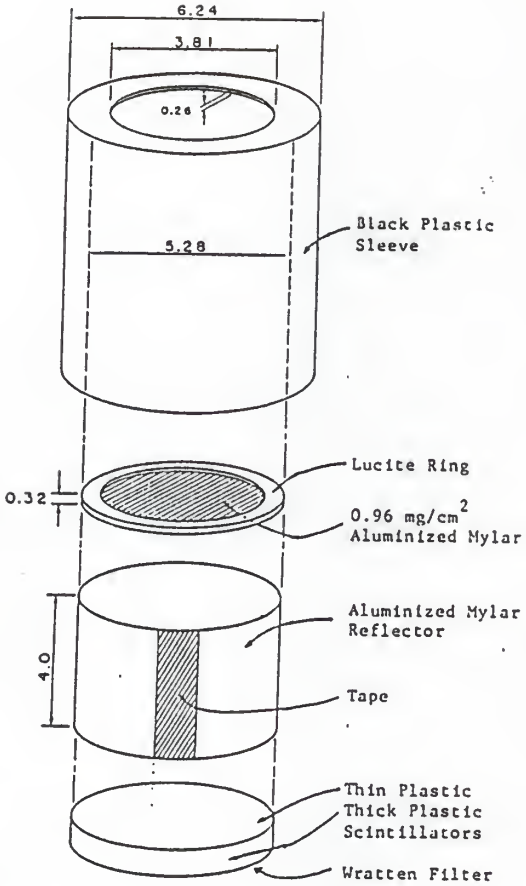

Fig. 3.5. Schematic diagram of a phoswich detector head for a beta-gamma spectrometer.

IV. PHOSWICH BETA-GAMMA SPECTROMETER SYSTEMS

A multitude of detector assemblies and associated electronic configurations were considered. The design objective was to discover workable combinations of detector assembly and associated pulse processing instruments. Configurations were selected and assembled from those that showed promise both from a practical standpoint based upon experience and from the results of limited mathematical modeling. Although there were many different pulse shape discrimination techniques to choose from, emphasis was placed upon the zero-crossing time technique. This time-to-amplitude based arrangement was found to be very convenient for researching the detector responses. As a consequence, most of the experimental data were acquired using this setup. Some data were also taken with a commercial pulse shape analyzer.

It was convenient to divide this discussion into two components--a brief theoretical description of phoswich voltage pulses and specific information on two of the phoswich spectrometers that were developed. The theoretical material is intended to demonstrate the potential that modeling has in helping to design a complex instrument. As was reported for the gas-filled proportional counter/plastic beta-particle spectrometer (Si85), the overall performance of a spectrometer depends upon the operating characteristics of the individual instruments. However, for that spectrometer, almost any combination of good quality instruments would work. This certainly is not true for phoswich detectors

because pulse shape discrimination requires much more exact control of the pulse shaping stages. The overall gamma-ray discrimination performance of these spectrometers not only strongly depended upon the impedance and design of a specific type of instrument but upon their specific settings, e.g., high voltage, shaping amplifier gain, and pulse shaping technique were all critical. Fortunately, once a specific instrument arrangement was established, data could be routinely measured without undue concern for long term instrument instability.

A. Theoretical Pulse Shaping Amplifier Waveforms

In Section III.C.2 the relative PMT charge, Q, was found for different combinations of scintillators, Wratten Gel filters, and the RCA 8575 PMT. The relative PMT charge determines the total PMT charge that will be produced per unit of absorbed radiation energy in a single scintillator. With this information, the amplitude of the voltage pulses produced by different pulse shaping amplifiers can be expressed more specifically. As in Section II.A.2 it is convenient to lump all of the factors which affect the pulse amplitude into a single term, I, and then treat subsequent shaping circuitry as affecting only the shape (time dependence) of the voltage pulse. Recall that the electron current in a PMT has the same time shape as the light scintillation current emitted from the phoswich detector.

$$i(t) = I_1(e^{-t/\tau_{d_1}} - e^{-t/\tau_{d_1}})$$

$$+ I_2 (e^{-t/\tau_{d_2}} - e^{-t/\tau_{r_2}}) , \qquad (4.1)$$

where the subscripts 1 and 2 refer to the top thin and bottom thick scintillators, respectively. I_1 and I_2 are given by

$$I_1 = E_1 Q_1/(\tau_{d_1} - \tau_{r_1})$$

$$I_2 = E_2 Q_2(\tau_{d_2} - \tau_{r_2}) , \qquad (4.2)$$

where E_1 and E_2 are the amount of radiation energy deposited in the thin and thick scintillators, and Q_1 and Q_2 are the relative total PMT charge produced in the PMT per unit of radiation energy absorbed in the thin and thick scintillator. The factors, $1/(\tau_{d_1} - \tau_{r_1})$ and $1/(\tau_{d_2} - \tau_{r_2})$, are required to ensure that for a unit of radiation energy deposited in either scintillator, the total PMT charge will equal Q. This factor was found by integrating the time dependent PMT current produced by a scintillator over time from 0 ns to infinity. The result must equal Q. Thus

$$Q E = \int_o^\infty i(t)\, dt$$

$$= \int_o^\infty I(e^{-t/\tau_d} - e^{-t/\tau_r})\, dt \qquad (4.3)$$

Evaluate the integral in Eq. (4.3), so that

$$Q\,E = I\left[-\tau_d e^{-t/\tau_d} + \tau_r e^{-t/\tau_r}\right]\Bigg|_{t=0}^{t=\infty}$$

$$= I(\tau_d - \tau_r) \; . \qquad (4.4)$$

Thus, I is given by

$$I = E\,Q/(\tau_d - \tau_r) \; . \qquad (4.5)$$

Refer to Section II.A.1 for a derivation of the amount of radiation energy, E_1 and E_2, absorbed by each scintillator for interactions with low energy beta particles, high energy beta particles, and gamma rays. Refer to Section III.C.2 for the calculated value of Q for various combinations of scintillators, filters, and the RCA 8575 PMT.

1. Linear Spectroscopy Amplifier

The linear spectroscopy amplifier is a powerful tool that serves as the interface instrument between the preamplifier output and the MCA input. This instrument, often called a linear amplifier, provides pulse shaping functions such as amplitude adjustment, rise and decay time, dc level, polarity, and pole zero cancellation. Pulses present at the input of an MCA must have the proper shape in order to satisfy the input specifications of commercial ADC circuits. All this is well known to the nuclear

instrument designer and user. However, optimal use of calculated waveforms, to help interpret the waveform that stems from the mixing of scintil-lation photons within the phoswich detector, is certainly not as well documented.

Normally, spectroscopy amplifiers are designed to amplify and shape the PMT linear tail pulse to provide a near Gaussian shaped linear voltage pulse with a maximum amplitude of 10 volts and a width of a few microseconds. The amplification of a well designed linear amplifier has negligible effect on the shape of the amplifier output waveform. Also, to a first approximation, the shaping circuit can be modeled as a single CR differentiator and n RC integrators connected in series. Figure 2.13 shows the equivalent circuit for the PMT along with a single CR-RC shaping circuit.

To model the output voltage from such a circuit, the input current must first be specified. The PMT current from a phoswich detector is given by Eq. (4.1). Refer to Fig. 2.13, showing the equivalent circuitry of the PMT and linear spectroscopy amplifier, and input the scintillation (or PMT) current from Eq. (4.1), and apply a Laplace transform method of solution to obtain the predicted output voltage pulse from a linear spectroscopy amplifier. Refer to Section II.C.6 for a complete derivation of the voltage pulse produced by this circuit.

Example voltage waveforms calculated for one phoswich configuration are shown in Fig. (4.1). The phoswich was a 0.5 mm-thick BC-444 on top of a thick (assumed thick enough to stop the

beta particles) BC-418 with a 1A Wratten Gel filter coupled to a RCA 8575 PMT. The circuit time constants were 100, 2000, and 2000 ns for the PMT equivalent circuit and the differentiator and integrator, respectively. These parameters are similar to those for one of the spectrometers which was assembled and studied extensively. As shown, beta-particle energies of 0.1 and 1 MeV and an electron energy of 1 MeV were selected. For Fig. 4.1A, the beta particle would be completely stopped in the thin scintillator. However, the 1 MeV beta particle (see Fig. 4.1B) would deposit energy in both scintillators. Under this condition, the equivalent of two voltage pulses would add to form the composite waveform. Finally, the single voltage pulse resulting from a gamma-ray interaction in the thick scintillator is shown in Fig. 4.1C. The distortion which is evident in the peak voltages would be even worse if the 1A filter was removed. (Compare the areas of Fig. 3.4.)

It should be emphasized that the waveforms calculated in this section are intended only as a guide. The accuracy of the equations used has not been determined. This requires further study. It is entirely possible however, that they may be suitable for all but the most stringent requirements.

2. Delay Line Shaping Amplifier

Delay line shaped waveforms were calculated for one specific type of commercial amplifier that was available in our laboratory--the ORTEC Model 460 Delay Line Amplifier. For purposes

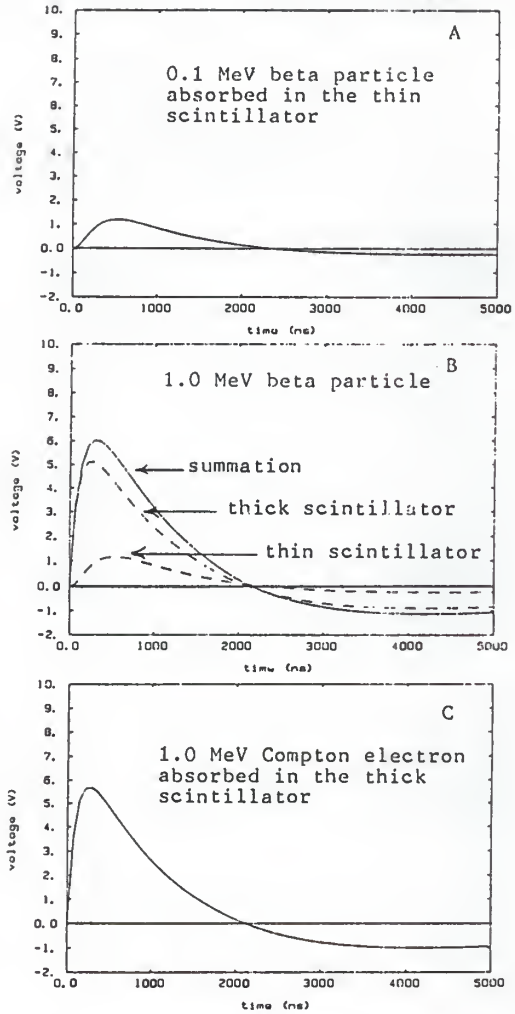

Fig. 4.1. Phoswich detector calculated voltage pulses shaped by a linear spectroscopy amplifier for three different radiation sources: (a) 0.1 MeV normally incident electron, (b) 1.0 MeV normally incident electron, and (c) 1.0 MeV Compton electron absorbed entirely by the thick scintillator.

of these calculations, we assumed that the circuit shown in Fig. 4.2 adequately described the pulse shaping features of this instrument. It was also assumed that the input of this instrument was connected directly to a low impedance PMT anode. All that was needed to derive the output voltage equation was to consider the PMT circuit, a single RC integrator and the function of a shorted delay line with a variable attenuator. The voltage pulse from the thin and thick scintillator can be summed to obtain the time-dependent voltage equations for the case where $RC_{PMT} \neq RC_1$. Thus for $0 < t < T_d$,

$$V_o(t) = (RC_1\, C_{PMT})^{-1} \sum_{j=1}^{2} I_j \left\{ \left[\frac{1}{RC_1} - \frac{1}{RC_{PMT}} \right]^{-1} \right.$$

$$\cdot \left[\left[\frac{1}{\tau_{d_j}} - \frac{1}{RC_{PMT}} \right]^{-1} - \left[\frac{1}{\tau_{d_j}} - \frac{1}{RC_{PMT}} \right]^{-1} \right] e^{-t/RC_{PMT}}$$

$$+ \left[\frac{1}{RC_{PMT}} - \frac{1}{RC_1} \right]^{-1} \left[\left[\frac{1}{\tau_{d_j}} - \frac{1}{RC_1} \right]^{-1} - \left[\frac{1}{\tau_{r_j}} - \frac{1}{RC_1} \right]^{-1} \right] e^{-t/RC_1}$$

$$+ \left[\left[\frac{1}{RC_{PMT}} - \frac{1}{\tau_{d_j}} \right] \left[\frac{1}{RC_1} - \frac{1}{\tau_{d_j}} \right] \right]^{-1} e^{-t/\tau_{d_j}}$$

$$\left. - \left[\left[\frac{1}{RC} - \frac{1}{\tau_{r_j}} \right] \left[\frac{1}{RC_1} - \frac{1}{\tau_{r_j}} \right]^{-1} e^{-t/\tau_{r_j}} \right] \right., \quad 0 < t < T_d \quad (4.6)$$

and for $t \geq T_d$,

$$V_o(t) = (RC_1\ C_{PMT})^{-1} \sum_{j=1}^{2} I_j \left\{ \left[\frac{1}{RC_1} - \frac{1}{RC_{PMT}} \right]^{-1} \right.$$

$$\left[\left[\frac{1}{\tau_{d_j}} - \frac{1}{RC_{PMT}} \right]^{-1} - \left[\frac{1}{\tau_{r_j}} - \frac{1}{RC_{PMT}} \right]^{-1} \right]$$

$$\cdot \left[e^{-t/RC_{PMT}} - f\, e^{-(t-T_d)/RC_{PMT})} \right]$$

$$+ \left[\frac{1}{RC_{PMT}} - \frac{1}{RC_1} \right]^{-1} \left[\left[\frac{1}{\tau_{d_j}} - \frac{1}{RC_1} \right]^{-1} - \left[\frac{1}{\tau_{r_j}} - \frac{1}{RC_1} \right]^{-1} \right]$$

$$\cdot \left[e^{-t/RC_1} - fe^{-(t-T_d)/RC_1} \right]$$

$$+ \left[\left[\frac{1}{RC_{PMT}} - \frac{1}{\tau_{d_j}} \right] \left[\frac{1}{RC_1} - \frac{1}{\tau_{d_j}} \right] \right]^{-1} \left[e^{-t/\tau_{d_j}} - fe^{-9t-T_d)/\tau_{d_j}} \right]$$

$$\left. + \left[\left[\frac{1}{RC_{PMT}} - \frac{1}{\tau_{r_j}} \right] \left[\frac{1}{RC_1} - \frac{1}{\tau_{r_j}} \right] \right]^{-1} \left[e^{-t/\tau_{r_j}} - fe^{-9t-T_d)/\tau_{r_j}} \right] \right\},$$

$$t \geq T_d\ , \qquad (4.7)$$

where the subscripts j=1 and j=2 refer to the slow and fast scintillator constants, respectively. Refer to Eq. (4.5) and Section II.A.2 for the equations used to determine the amplitude of I_1 and I_2 for gamma-ray Compton electrons, low energy beta particles, and high energy beta particles. Note that, expressed in

this manner, the output voltage is a composite waveform, consisting of a slow scintillation component, and a fast scintillation component. Figure 4.3 shows the waveforms calculated using Eq. (4.7) for 0.1 and 1 MeV beta particles and 1 MeV Compton electrons. The circuit parameters were: RC_{PMT} of 100 ns, integration time constant of 250 ns, and delay of 250 ns. The variable attenuation factor (f) was set equal to one. The difference in zero-crossing time is clearly evident between the beta particles and the gamma-ray Compton electron.

3. Timing Filter Amplifier

A fast timing filter amplifier with pulse shaping circuitry consisting of a single differentiator and integrator was modeled. This instrument was very similar to the spectroscopy amplifier described in Part 1 except the RC time constants are of the order of a few ns. These fast time constants help preserve the timing information of the PMT output pulse, while providing a pulse that has a useful amplitude. Figure 4.4 shows the output pulses calculated for 0.1 and 1 MeV beta particles and Compton electrons that are stopped in the thick (fast) scintillator. System parameters for this case were: RC of 100 ns and equal differentiation and integration time constants of 20 ns.

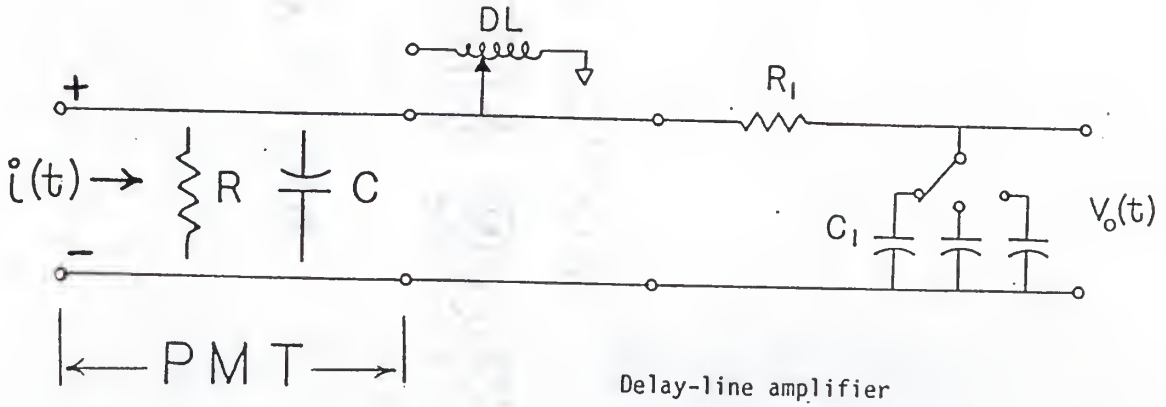

Fig. 4.2. Schematic circuit diagram of the shaping circuitry of the ORTEC Model 460 delay line shaping amplifier connected to the photomultiplier tube.

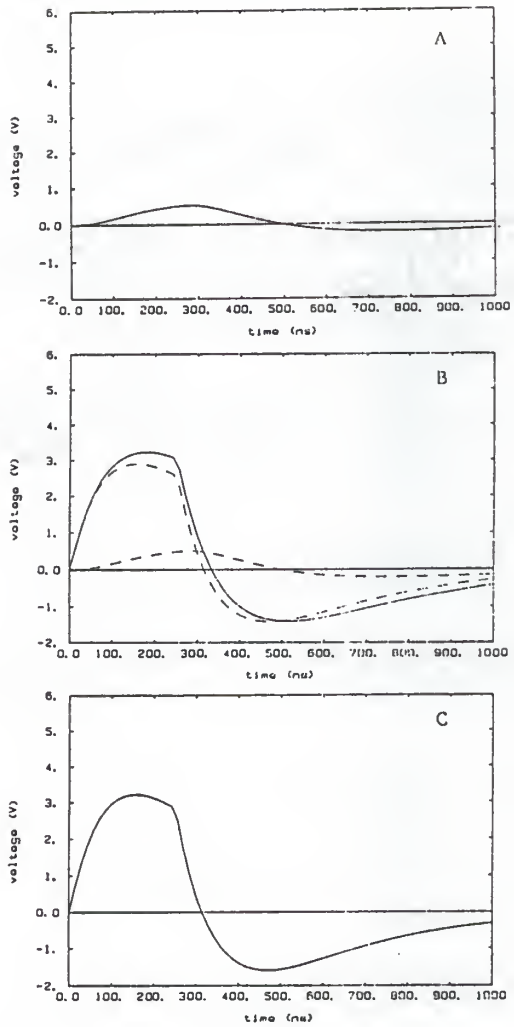

Fig. 4.3. Phoswich detector calculated voltage pulses shaped by a delay line shaping amplifier for three different radiation sources: (a) 0.1 MeV normally incident electron, (b) 1.0 MeV normally incident electron, and (c) 1.0 MeV Compton electron absorbed entirely by the thick scintillator.

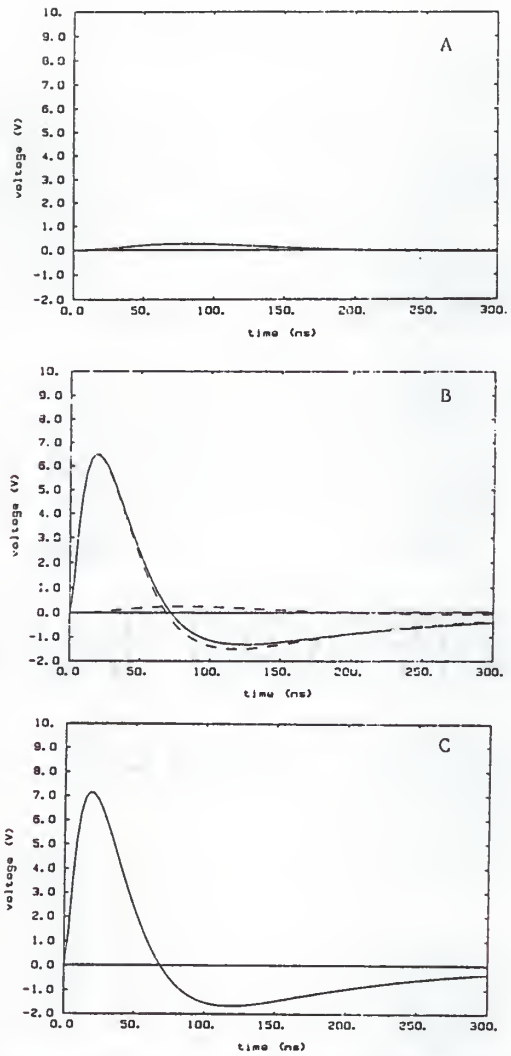

Fig. 4.4. Phoswich detector calculated voltage pulses shaped by a fast timing filter amplifier for three different radiation sources: (a) 0.1 MeV normally incident electron, (b) 1.0 MeV normally incident electron, and (c) 1.0 MeV Compton electron absorbed entirely by the thick scintillator.

B. Zero-Crossing Time Associated Electronics

A popular pulse shaping technique, called zero-crossing time, is based upon forming a voltage pulse whose zero crossing time is proportional to the pulse decay time. By generating two timing signals, a fixed reference time signal and the zero-crossing signal, it is then possible to establish a new voltage pulse whose amplitude is proportional to the decay time of the original shaped PMT signal (see Fig. 4.5). Moreover, it is possible to perform pulse shape discrimination nearly independent of the pulse amplitude. An early gamma-ray discrimination application applied to neutron spectroscopy was reported by Alexander and Goudling (A161). They found that if they integrated the detector current and then performed double differentiation a desirable zero-crossing voltage pulse was formed. This technique, and many related methods (Ho67, Ka70, Ta70, Wi72, Bo72, Sh72, Sy72, and Ah77) all fall into the category of zero crossing since they are based upon forming a voltage pulse whose zero-crossing time is proportional to the decay time.

The zero-crossing time method depends very much on how the PMT output current is processed to form the zero-crossing voltage pulse. The phoswich spectrometer assembled which used the zero-crossing principle is shown in the block diagram of Fig. 4.6. Pulse processing for particle identification was performed on the anode signal starting with the preamplifier. This preamplifier was direct coupled, had a voltage gain of 10, a fast rise time of 1.5 ns, and had an input and output impedance of 50 ohms. One of the most

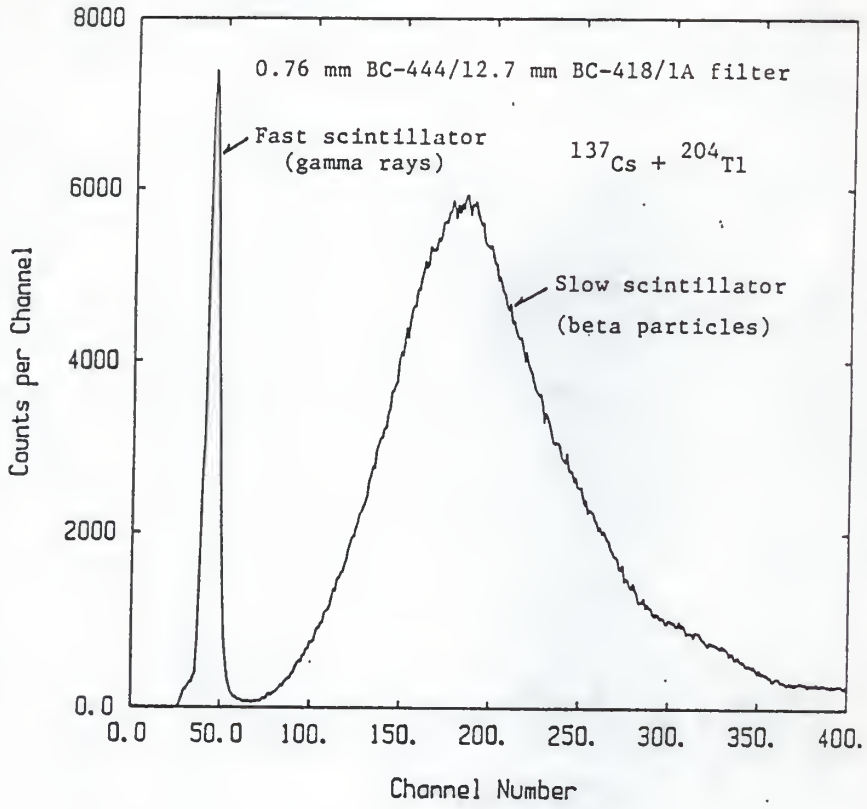

Fig. 4.5. Gamma ray and beta particle time distribution determined by measuring the zero crossing time of a phoswich detector delay line shaping amplifier output.

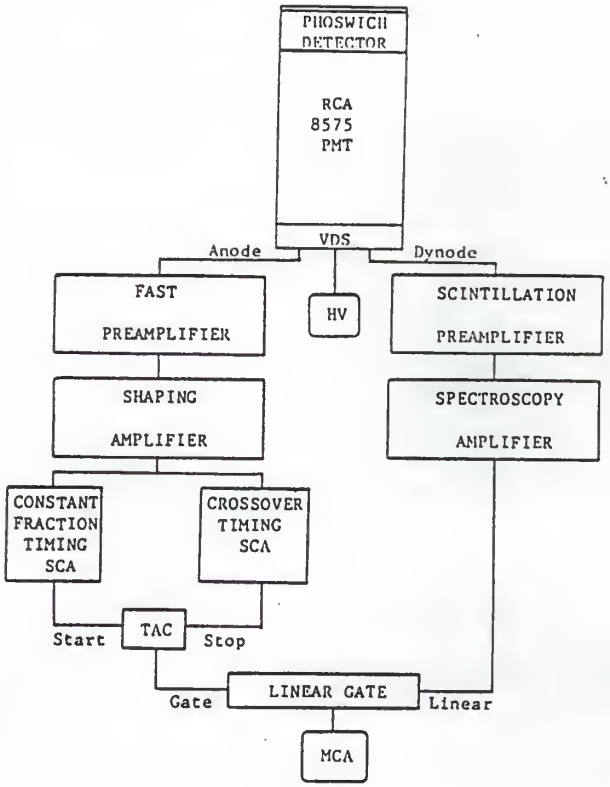

Fig. 4.6. Block diagram of the KSU Phoswich beta-particle spectrometer with active gamma ray discrimmination using the zero-crossing time technique.

important shaping components was the shaping amplifier. Several commercial instruments were tested. It was found that the best data, for our studies, were obtained using either a delay-line amplifier or a timing-filter amplifier. The delay-line amplifier was well suited for this timing application because of rapid recovery from large overload pulses and small crossover walk over a large dynamic range. An amplifier with 250 ns delay lines, an integration time constant of 250 ns, and a gain of 60 was employed in a number of our beta-particle pulse height measurements. Unless otherwise noted, the data presented in this report were acquired with this delay-line amplifier.

C. Pulse Shape Analyzer

A commercial PSA (Pulse Shape Analyzer) was also tested which measured the fall time of the input pulse from the shaping amplifier and generated a linear output with an amplitude that was proportional to the fall time (the general operational information presented in this section is based upon descriptive material presented in the ORTEC Model 458 Pulse Shape Analyzer Operating Manual). These phoswich detector output pulses were analyzed directly with a multichannel analyzer to determine the pulse decay time distribution (see Figs. 4.7-4.9). It also includes a single channel analyzer that generated two logic output pulses, based on the measured fall time. One of the single channel logic outputs corresponded to pulses with the longer decay times and occurred when

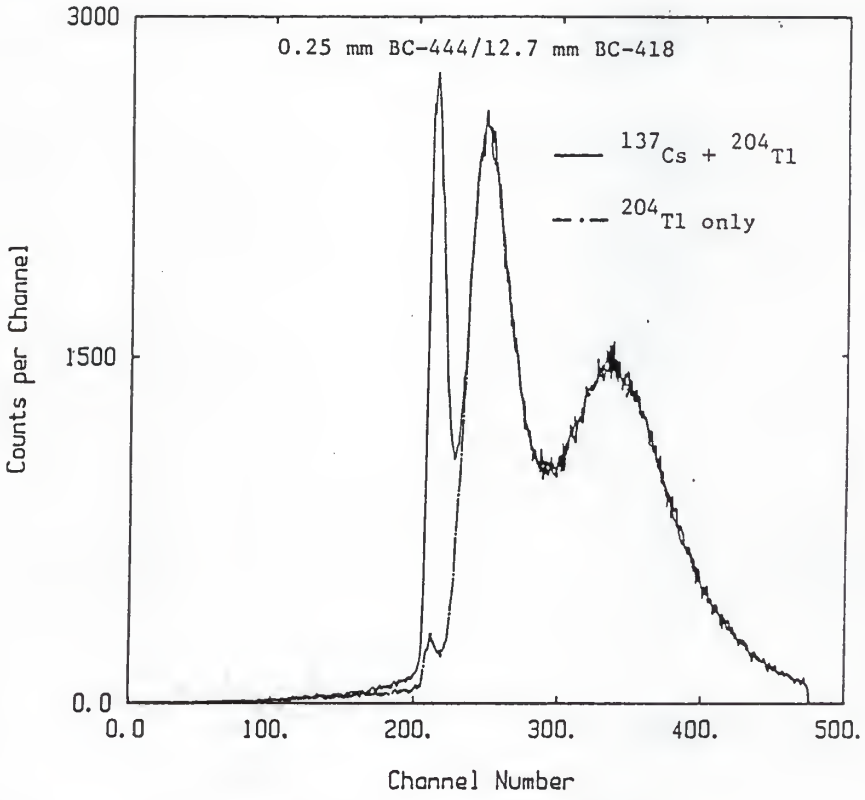

Fig. 4.7. Time distribution curve of a phoswich detector exposed to Cs-137/Ba-137m gamma rays and Tl-204 beta particles generated using a commercial pulse shape analyzer.

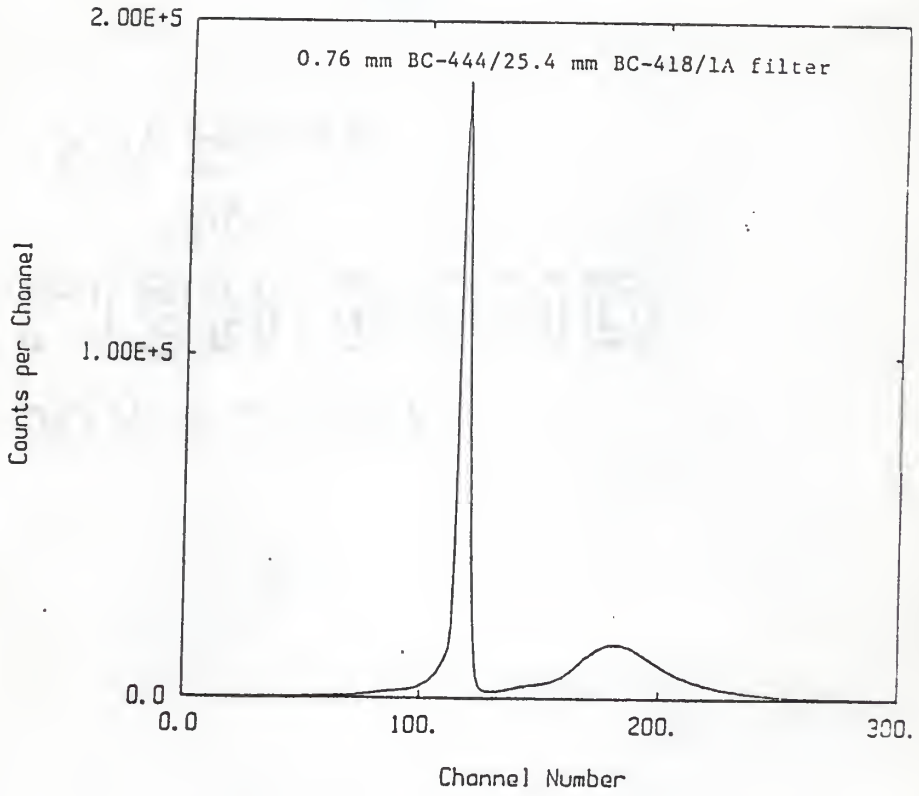

Fig. 4.8. Time distribution of mixed field Cs-137/Ba-137m and Tl-204 radiation measured with a commercial pulse shape analyzer.

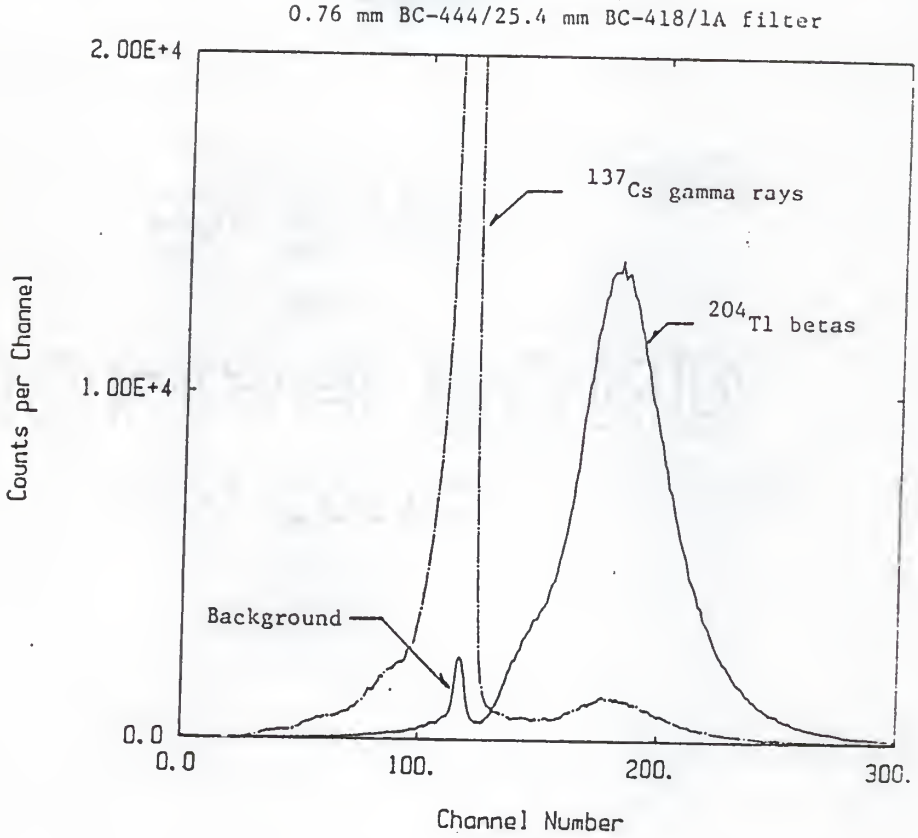

Fig. 4.9. Enhanced scale view of the time distribution of Cs-137/Ba-137m gamma rays and Tl-204 beta particles measured with a commercial pulse shape analyzer.

the upper level time setting was exceeded. A separate logic output occurred when the amplitude of the pulse generated fell between a lower and an upper level time window. Moreover, a third logic pulse was available which was generated each time the input voltage pulse exceeded the input discriminator level setting.

As shown in Fig. 4.10, this NIM module accepted the input pulses from the shaping amplifier. Therefore, the associated electronics selected played an important role in the overall performance of the spectrometer when the PSA was utilized. Spectrometer systems containing this instrument were constructed and their performance evaluated.

D. Pulse Shape Discrimination Timing

Beta-particle acceptance is accomplished by requiring coincidence between the beta sensor detector and the total energy absorption detector. In the absence of a slow pulse component stemming from ionization in the thin beta sensor detector, any ionization within the thick detector is assumed to be caused by a gamma ray and is disregarded. General timing information is presented in Fig. 4.11 for the zero-crossing time technique. Once the PMT anode output signal has passed the timing test set for beta particles, a positive logic output pulse appears at the TAC SCA output. At this time, the timing operation of this zero-crossing spectrometer is the same as that of both the phoswich with the PSA

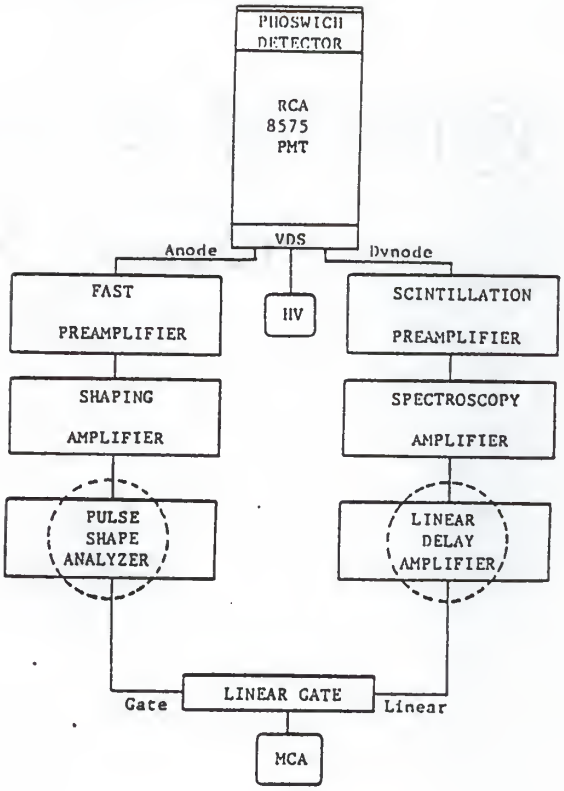

Fig. 4.10. Block diagram of the KSU phoswich beta-particle spectrometer with active gamma-ray discrimmination using a commercial pulse shape analyzer.

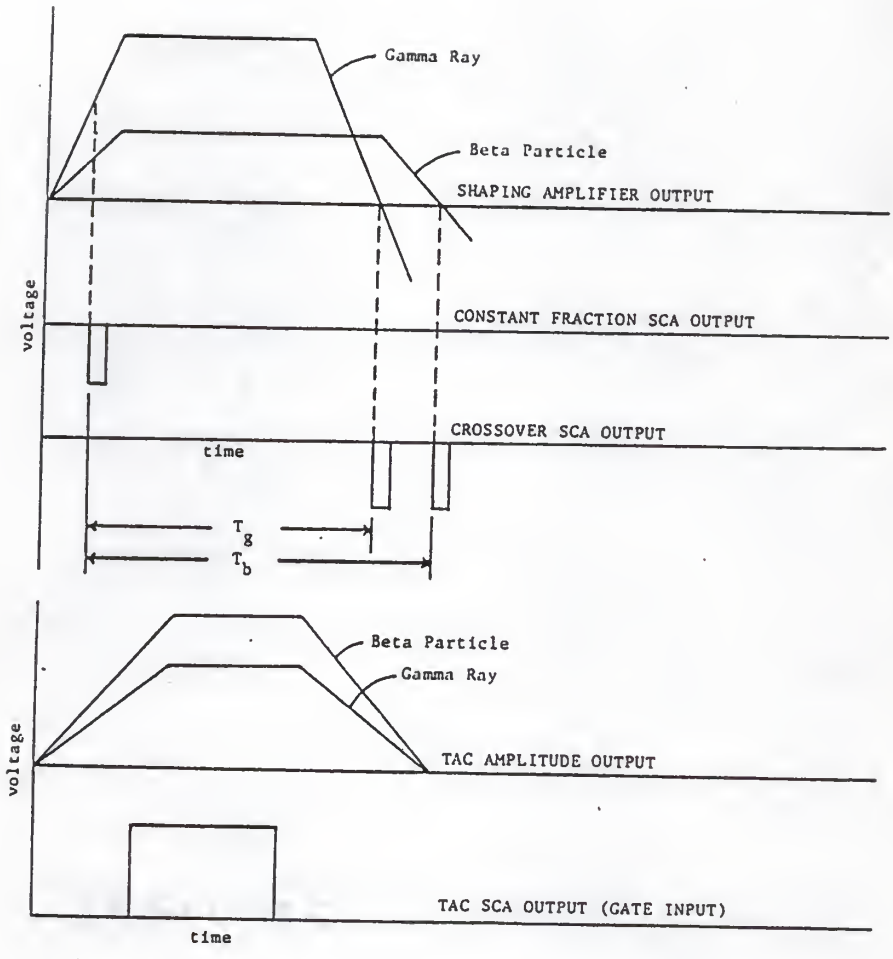

Fig. 4.11. Timing diagram for the zero-crossing-time generated gate input pulse signaling the interaction of a beta particle in the phoswich detector.

module and the previously developed gas-flow proportional/plastic scintillator spectrometer (Si85).

Timing operations depend upon both the type of data to be acquired and the operating features of the linear gate. The following description assumes that it is desirable to independently measure three different types of pulse height distributions: 1) beta particles and electrons only; 2) gamma rays only, and 3) the combination of these two. In addition, pulse pileup at high count rates is to be reduced relative to straight pulse conversion. The operation of the specific linear gate module used here is different than that of a standard linear gate. An overview of the features important to the coincidence operation of the spectrometer is presented in terms of the five pulses shown in Fig. 4.12. These include the two input signals, the linear gate OUTPUT pulse, the BUSY OUTPUT pulse and the GATE PERIOD pulse (another internally generated signal). The GATE pulse shown in Fig. 4.12A is present only if radiation induced ion pairs are produced in the active volume of the thin beta sensor. This is a standard positive NIM logic pulse. When the linear gate module is set for coincidence operation, the GATE input signal must occur before the peak amplitude of the LINEAR input signal. Otherwise, the OUTPUT pulse amplitude will not be proportional to the amplitude of the LINEAR input. To assure that this condition was satisfied, even when the walk in this timing signal was considered, the GATE was set to occur at approximately the time of arrival of the LINEAR pulse. The

LINEAR input signal, from interactions within the thick plastic scintillator, is set to arrive at the time shown in Fig. 4.12B. When the amplitude of this signal exceeds the discriminator (LLD) threshold, the presence of the signal will be sensed only if the busy circuit has been reset. If the previous signal has not been processed, then pileup effects are automatically decreased by waiting for the next signal which occurs after the busy circuit has reset. In addition, the input signal will be rejected if: 1) the output pulse has not been completed, 2) the operating mode is GATED/COINC and a GATE signal was not present or 3) the operating mode is GATED/ANTI COINC and a GATE signal was present and the GATE PERIOD is still in effect. If, however, the busy circuit has reset, the LINEAR input signal exceeds the discriminator level, the GATE signal has arrived, and the mode is GATED/COINC the GATE PERIOD signal initiated has a start time in coincidence with the leading edge of the GATE signal and a user determined width. The GATE PERIOD signal must continue beyond the internal detection of the LINEAR signal peak amplitude. For proper operation of the spectrometer in both the GATED/COINC and the GATED/ANTI COINC modes, the pulse width was set at about 5 μs (see Fig. 4.12C). If the peak amplitude has been detected and the GATE PERIOD is set, a BUSY output signal is generated. As shown in Fig. 4.12D, its duration is about 2 μs. The duration is determined by the time elapsed from the time the LINEAR signal peak amplitude is determined until the OUTPUT has been furnished and the discriminator is reset. An additional

user adjustment is the width of the OUTPUT pulse. This width, independent of the width of the input pulse, was set as shown in Fig. 4.12E at 1.5 μs. For GATED/ANTI COINC operation, the GATE PERIOD must overlap the period of discriminator response to any LINEAR pulse that is to be inhibited by the GATE signal. This is the reason that the GATE PERIOD was set at a maximum.

In summary, to measure beta particle or electron pulse height distributions, select the GATED/COINC mode. For gamma rays only, operate in the GATED/ANTI COINC mode. In the NORMAL mode, the GATE signal has no effect on the OUTPUT and the pulse height distribution is the electron distribution stemming from a combination of beta particle, electron, or gamma ray interactions in the thick organic scintillator.

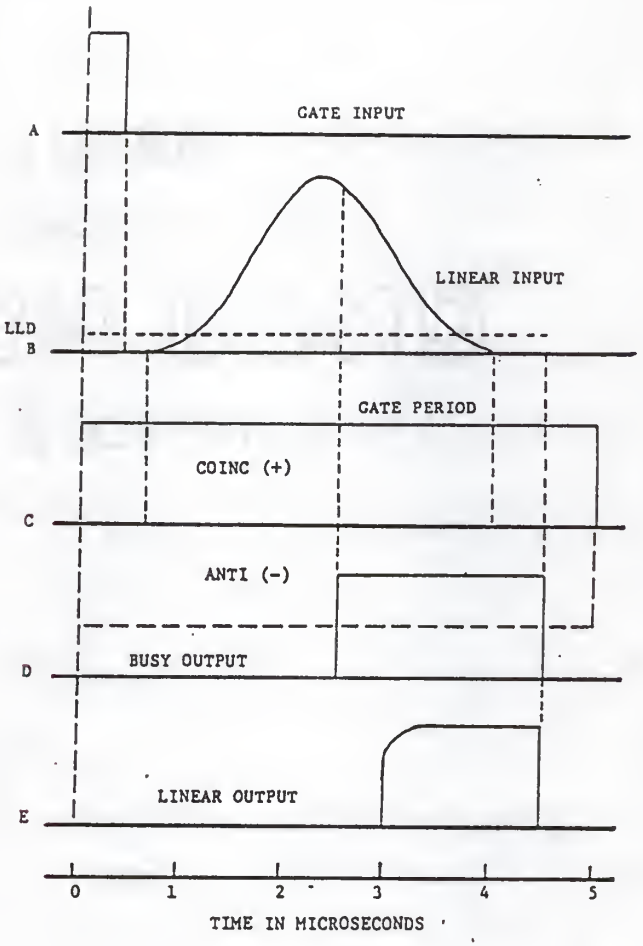

Fig. 4.12. Timing diagram for the linear gate triggered by beta particle induced gate input signal formation from the phoswich detector and associated electronics.

V. RESULTS AND CONCLUSIONS

The final test of the previously developed models and equations is how closely the predicted or calculated voltage waveforms match actual measured voltage waveforms produced by commerical PSD circuitry. In Section II.A, an empirical relation was introduced to characterize the time-dependence of the light scintillation current that is produced by the phoswich detector for gamma-ray Compton electrons, low energy beta particles, and high energy beta particles. In Section II.B, the PMT voltage waveform produced by scintillation in the phoswich detector was derived. Section II.C went on to derive the voltage waveforms produced by pulse shaping circuit components commonly found in commercial PSD equipment. All of this was combined in Section IV.A to predict the voltage waveforms produced by commerical linear spectroscopy amplifiers, delay line shaping amplifiers, and timing filter amplifiers. The equations developed in Section IV.A are very general, and can be used to predict the output voltage waveforms produced by the above mentioned commerical PSD instruments for any combination of thin scintillator, thick scintillator, Wratten Gel optical filter, PMT, and adjustable setting of commercial PSD instruments.

The derived voltage waveform equations are not intended to predict the exact voltage waveforms that would be observed in actual laboratory experimentation. Rather, they are intended to provide a very close approximation of the voltage waveforms that would be observed in the laboratory. Recall that the derivation

of the predicted voltage waveforms assumed ideal behavior propeties of the organic scintillator, PMT, and circuit components of commercial PSD instruments. In actuality, several factors will cause distortions between the actual and predicted voltage waveforms. Among these factors are afterglow (delayed phosphorescence) by the organic scintillators, statistical time spread of the electron current pulse during amplification by the PMT, stray capacitance and impedance in the PMT and PSD circuitry, accuracy of the manufacturers specifications, and special circuitry, such as circuit protection or noise reduction circuitry. The only variables contained in the predicted voltage waveform equations are the characteristic time constants of the organic scintillators (τ_d and τ_r), PMT (RC_{PMT}), differentiator(s) and/or integrator(s) (RC_i), and delay line (T_d). Therefore, it may be necessary to adjust one or more of these characteristic time constants so that the predicted voltage waveform equations closely match the actual observed laboratory voltage waveforms for a given PSD system. It is easy to realize the benefit that a simple, yet accurate model of the actual laboratory measured voltage waveform could provide to the PSD system designer. This model would enable the PSD system designer to quickly predict the voltage waveform response to the many permutations of scintillator, Wratten Gel optical filter, PMT, and connected PSD instruments with variable settings. It is important to be able to easily predict the voltage waveforms, because the total PSD system performance (gamma discrimination ratio, maximum

discrimination energy, and linearity between radiation energy and assigned MCA channel number) depends upon the actual voltage waveforms produced by the PSD system when exposed to a mixed beta-particle and gamma-ray field. Only a few laboratory measurements are necessary to determine the characteristic time constants of the PSD system parameters (some of which are adjustable). For example, the manufacturers specified equivalent RC time constant for a PMT may be 100 ns, but better agreement between the laboratory measured PMT voltage waveform and the predicted voltage waveform equation may be obtained by using 120 ns as the PMT RC time constant. (Usually, the pre-amplifier is considered to be part of the PMT's RC time constant.) Using these modified time constants, the PSD system designer can use computer modeling to quickly determine the optimum PSD system that can be obtained with actual instruments that are available, and avoid much of the laboratory experimentation otherwise necessary. The method recommended and used for determining the best value of the PSD system parameters is described here.

First, obtain the necessary PSD system components. Obtain a monoenergetic electron source and a gamma-ray source with an easily identifiable energy. Obtain the Wratten Gel optical filters which preliminary results suggest may be useful (Refer to Section III.B) and obtain fast and slow organic scintillators of sufficient thickness to completely stop the mono-energetic electron. The scintillators should all have the same thickness. Obtain a PMT

with fast timing properties. Fast timing properties (short RC time constant) are necessary to preserve the timing information from the two scintillators. Now, an oscilloscope tracing of the output voltage pulse from the PMT (or preamplifier) can be used to determine the values of the scintillator and PMT time constants. Place a scintillator of interest on the photocathode of the PMT. Expose the scintillator to the monoenergetic electron source, and determine the best-fit value of τ_d, τ_r, and RC_{PMT} for the PMT voltage pulse given by Eq. (2.19). Repeat for all scintillators. Note that RC_{PMT} should not change for different scintillators.

Second, determine the relative PMT charge produced by each combination of scintillator and organic filter. Connect the output of the PMT to a linear MCA system that has 1024 or more channels. Place the scintillator with the greatest light output on the photocathode of the PMT. Adjust the gain of the linear spectroscopy amplifier so that mono-energetic electron interactions are recorded in a high channel of the MCA. Do not change the gain of the linear amplifier or the setting of the PMT high voltage during this section, or the results will be invalid. Record the channel number that the mono-energetic electrons are recorded in. Now place a Wratten-Gel optical filter of interest between the scintillator and photocathode of the PMT (see Section III.E). Record the channel number that mono-energetic electrons are now recorded in. The relative PMT charge between the scintillator without filter, and scintillator plus filter is simply the ratio of channel numbers.

Repeat for all filters of interest. Next, without changing the gain settings, place another scintillator of interest on the photocathode of the PMT. Record the channel number that the mono-energetic electron interactions are recorded in. The ratio between this channel number and the channel number recorded for the first scintillator is the ratio of PMT charge produced by these scintillators. Next, as before, insert Wratten-Gel optical filters of interest to find the relative PMT charge produced by each combination of scintillator and filter of interest.

The last step is to determine the characteristic RC time parameters of commercial PSD instruments that are to be connected to the PMT voltage output. To do this, connect the PSD instrument, set it to the first setting of interest, and examine the output voltage pulse. Leaving the scintillator and PMT time constants as determined in the first step, determine the best value of the RC time constant(s) for the predicted voltage waveform equation that describes the PSD instrument used.

The above described method was used at KSU and the results are given in the following sections for a BC-444 thin scintillator, a BC-418 thick scintillator, a Kodak 1A Wratten Gel optical filter, EG&G ORTEC Model 460 Delay Line Amplifier, TENNELEC TC203BLR linear spectroscopy amplifier, and a ^{137}Cs radiation source.

A. Characteristic Time Constants of the Scintillator and PMT.

The electron source was placed 4 inches above the 0.5 inch thick BC-418 scintillator. The oscilloscope (Tektronix Model 475) was connected to the EG&G ORTEC Model 9301 fast preamplified anode output of the PMT (RCA-8575). The output voltage waveform was recorded by digitizing a sketch of the oscilloscope tracing using the computer code "PCDIGI" developed at KSU. Next, the BC-418 scintillator was taken off and replaced with the BC-444 scintillator. The digitizing procedure was repeated to digitize the resulting output voltage waveform. Then the parameters τ_d, τ_r and RC_{PMT} in Eq. (2.19) were adjusted by trial and error until excellent agreement was observed between the oscilloscope measured waveform, and the predicted voltage waveform of Eq. (2.19). The MCA input is obtained from a slow shaping preamplifier (EG&G ORTEC Model 113) connected to the last dynode output of the PMT. This pre-shaping before the linear spectroscopy amplifier provides a more desirable voltage waveform input to the linear spectroscopy amplifier. The equivalent RC_{PMT} time constant of the PMT and slow shaping preamplifier was determined similar to the fast preamplifier-PMT procedure described above. A trial and error estimation of the parameters was used, because any estimates from statistical curve fitting routines would have been accepted only if they seemed to match closely with measured waveforms for three critical requirements: rise time (time to increase from 10% of peak height to 90% of peak height), voltage peak (amplitude and time at which

peak occurs) and decay time (time to decrease from 90% of peak height to 10% of peak height). It would have been difficult to numerically optimize according to these three parameters. The characteristic value of the parameters τ_d and τ_r for each scintillator is listed in Table 5.1. The characteristic value of RC_{PMT} for the fast and slow preamplifier output is also listed in Table 5.1. Refer to Figs. 5.1 and 5.2 for a comparison between the measured PMT preamplifier voltage waveforms and the predicted voltage waveforms using these parameters for the BC-444 and BC-418 scintillators.

B. Relative PMT Charge for Scintillators and Filter Combinations

The electron source was placed 4 inches above the 0.5 inch thick BC-418 scintillator. The linear spectroscopy amplifier shaping time constants were set on 2 μs. The gain was adjusted so that the electron interactions were recorded in channel number 819, with a scale of 0-1023 channels. Then the 1A Wratten Gel filter was inserted between the scintillator and the photocathode of the PMT. Electron interactions were observed shifted to channel 354. Next the 0.5 inch thick BC-444 scintillator was placed on the PMT. Electron interactions were recorded in channel 650. With the 1A filter inserted between the BC-444 scintillator and the PMT, electron interactions were recorded in channel 539. The channel number corresponding to the electron interactions were normalized relative to the BC-418 scintillator without the 1A filter. These results are listed in Table 5.1.

Table 5.1. Laboratory measured best-fit parameters for the scintillators, 1A Wratten Gel filter, RCA 8575 PMT, TENNELEC TC 203BLR linear spectroscopy amplifier, and ORTEC Model 460 delay line shaping amplifier.

SCINTILLATOR

	Time Constants (ns)		Relative PMT Charge	
	τ_d	τ_r	with filter	without filter
BC-444	210	20	66	79
BC-418	4.5	3	43	100

PMT-PREAMPLIFIER

	RC Time Constant (ns)
Fast Preamplifier	8
Slow Shaping Preamplifier	40,000

DELAY LINE SHAPING AMPLIFIER

	Instrument Setting (ns)	Best-Fit Estimate (ns)
Delay Time	250	250
Integration RC Time Constant	250	400

LINEAR SPECTRSCOPY AMPLIFIER

	Instrument Setting (ns)	Best-Fit Estimate (ns)
Differentiation RC Time Constant	2000	2500
Integration RC Time Constant	2000	2500

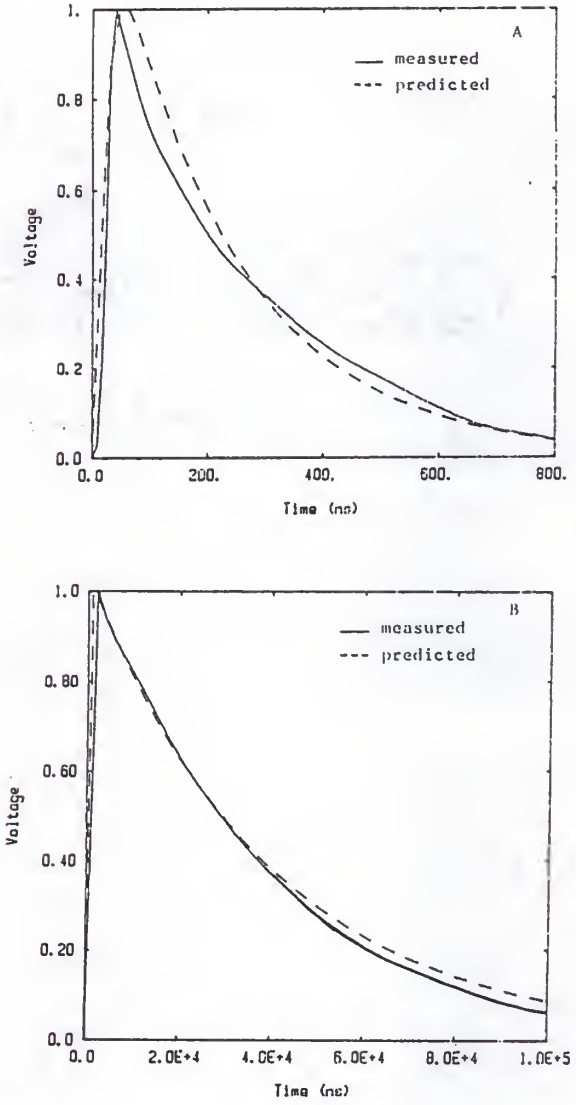

Fig. 5.1. A comparison of the BC-444 scintillator PMT measured and predicted voltage waveforms using the parameters given in Table 5.1 for (a) the fast pre-amplifier output, and (b) the slow shaping preamplifier output.

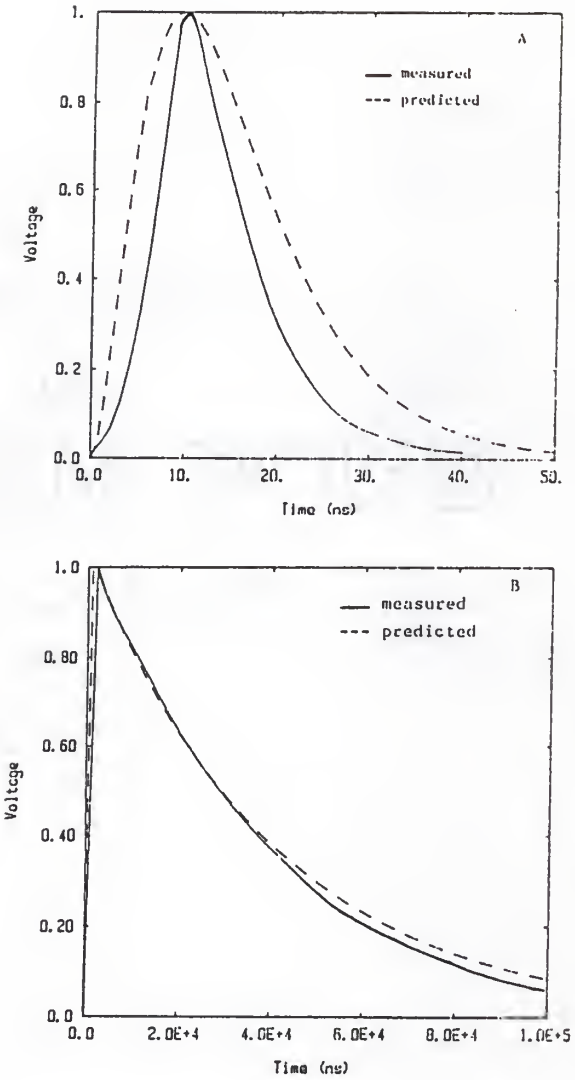

Fig. 5.2. A comparison of the BC-418 scintillator PMT measured and predicted voltage waveforms using the parameters given in Table 5.1 for (a) the fast pre-amplifier output, and (b) the slow shaping preamplifier output.

C. Linear Spectroscopy Amplifier Voltage Waveforms

Next, the linear spectroscopy amplifier (Tennelec TC 203BLR) was connected directly to the slow shaping pre-amplifier (EG&G ORTEC Model 113) output. The adjustable RC time constants of the linear amplifier were set to 2 μs. The BC-444 scintillator was placed on the photocathode of the PMT. As before, the voltage waveform was observed with the oscilloscope connected to the linear spectroscopy amplifier output. The oscilloscope tracing was used to digitize the output voltage waveform. This procedure was repeated with the BC-418 scintillator placed on the photocathode of the PMT. Then, using the previously found value of the parameters τ_d, τ_r and RC_{PMT}, the best-fit values of the linear spectroscopy amplifier integration and differentiation time constant in Eq. (2.82) were determined and are listed in Table 5.1. Refer to Figs. 5.3 and 5.4 for the comparision between the measured and predicted linear spectroscopy amplifier voltage waveforms.

D. Delay Line Shaping Amplifier Voltage Waveforms

The delay line shaping amplifier (ORTEC Model 460) was connected to the PSD system as diagrammed by Fig. 4.6. The delay line time constant was factory set to 250 ns, a value which preliminary investigations suggested would provide the best results of all of the delay time constants commercially available for this instrument. The RC integration time constant was set to 250 ns. After comparing the measured and predicted voltage waveforms using

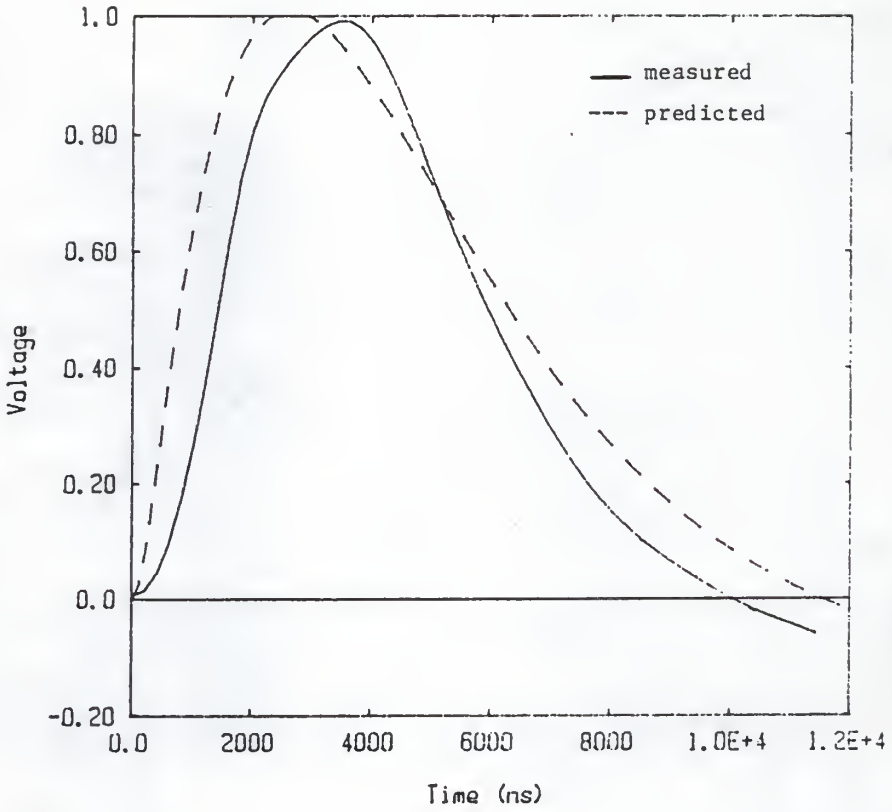

Fig. 5.3. A comparison of the BC-444 linear spectroscopy amplifier measured and predicted voltage waveforms using the best-fit parameters given in Table 5.1.

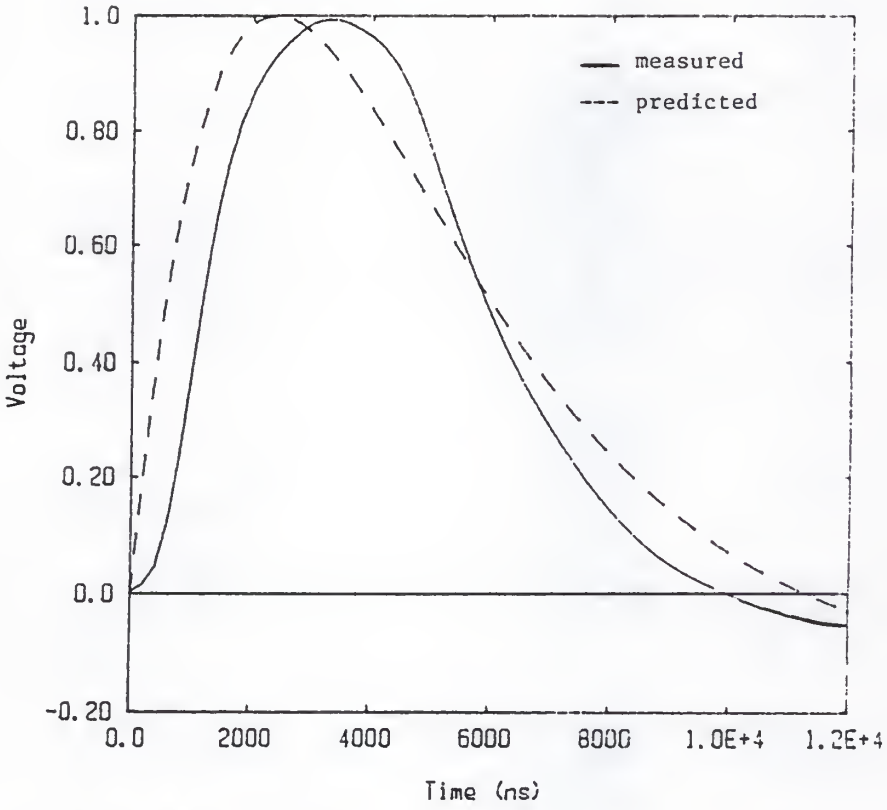

Fig. 5.4. A comparison of the BC-418 linear spectroscopy amplifier measured and predicted voltage waveforms using the best-fit parameters given in Table 5.1.

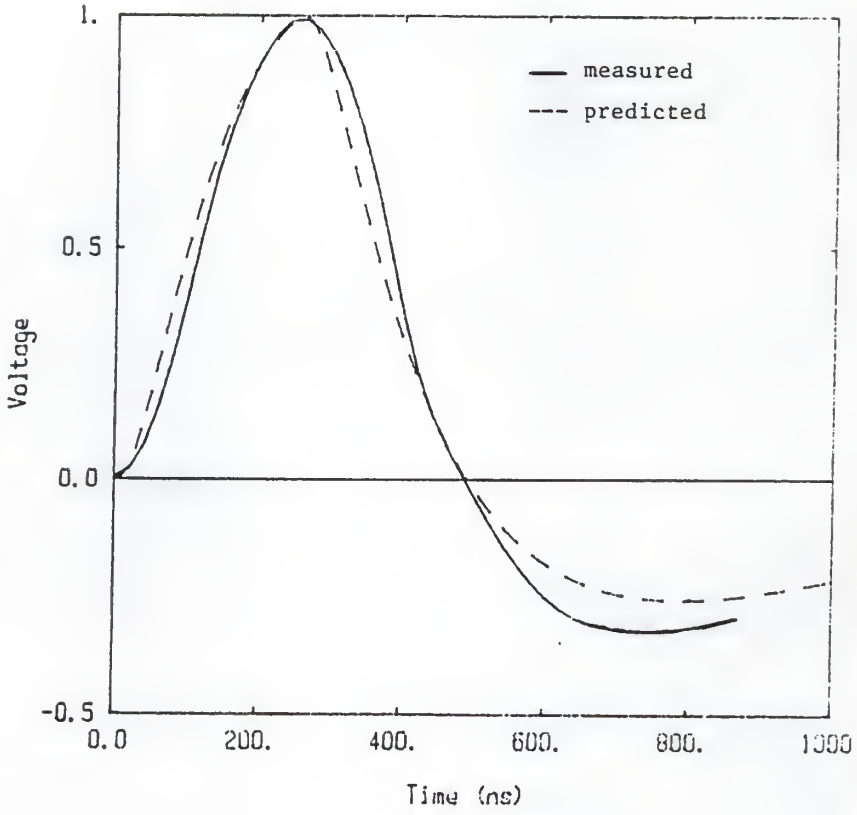

Fig. 5.5. A comparison of the BC-444 delay line shaping amplifier measured and predicted voltage waveforms using the best-fit parameters given in Table 5.1.

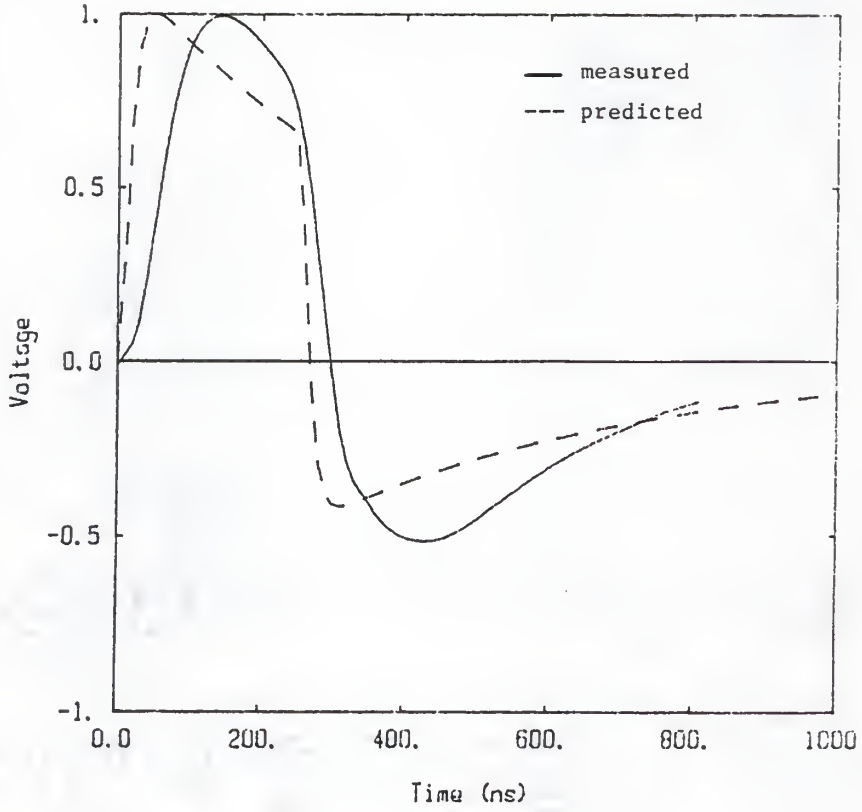

Fig. 5.6. A comparison of the BC-418 delay line shaping amplifier measured and predicted voltage waveforms using the best-fit parameters given in Table 5.1.

Eqs. (4.6) and (4.7), the best-fit value of delay time T_d, and integration time constant was determined. These values are listed in Table 5.1. Refer to Figs. (5.5) and (5.6) for a comparison between the measured and predicted delay line shaping amplifier voltage waveforms for the BC-444 and BC-418 scintillators.

E. General Observations of the Voltage Waveforms

An overall good agreement was found between the laboratory measured voltage waveforms, and the predicted voltage waveforms using the estimated parameters found in Table 5.1. It was difficult to accurately digitize many of the laboratory measured waveforms, due to several factors. Compton electrons from the $^{137}Cs/^{137m}Ba$ source interferred with ^{137}Cs mono-energetic electron (which has energy slightly greater than the maximum ^{137m}Ba Compton electron) and created a "pile-up" of amplitudes on the oscilloscope tracing. Though the shapes of all amplitude were the same, it was difficult to observe the exact tracing of a single pulse on the oscilloscope screen. Digital storage oscilloscopes available can store pulse information at a rate of only 0.5 μs per point. This was just not fast enough for most of the voltage waveforms studied here. However, the oscilloscope tracing was clear enough to determine the time at which maximum or minimum amplitudes and zero-crossover occurred, and the general shape of the voltage waveform. From examining Figs. (5-1) to (5-6), it seems that some of the laboratory measured waveforms are time-shifted from the predicted voltage

waveforms. This systematic time shift may be attributed to experimental error of interpreting the starting point of the waveform registered on the oscilloscope screen.

VI. SUGGESTIONS FOR FURTHER STUDY

The equations developed in this report were intended to assist the PSD system designer by providing a means to predict the effect that the many adjustable variables would have on the overall performance characteristics of a particular phoswich detector beta-gamma spectroscopy system. Although it was shown that these equations could closely model the laboratory measured voltage waveforms, the accuracy of these equations was not determined.

The amount of radiation energy that a beta particle or gamma ray will deposit in each scintillator (and hence total light output from each scintillator) is extremely important to know in order to fabricate the individual scintillators to the optimum thickness. The optimum thickness of each scintillator varies greatly depending on the maximum energy for which discrimination is desired, the minimum scintillator light output that is necessary to exceed the noise level, and the relative fraction of the top thin scintillator light output compared with total light output that is necessary for the discrimination circuitry to sense that a slow component is present. The equation used for this report to predict the energy deposited in each scintillator was an empirical, statistical formula. Greater accuracy for calculating the optimum thickness of each scintillator could be obtained by using Monte Carlo calculations which could account for the individual behavior (random scattering angle) of beta-particle and gamma Compton electrons. These Monte Carlo methods could also provide the maximum gamma-

discrimination ratio that is physically possible for a phoswich detector in a mixed radiation field. The performance of the PSD system could then be evaluated by comparison with the physical limit. The energy dependence of discrimination could also be predicted.

VII. ACKNOWLEDGEMENTS

I would like to express my sincere appreciation to Dr. G. G. Simons for the help, guidance, and insight that he provided to me during the research of this project and preparation of this thesis.

I would also like to thank the faculty and staff of the KSU Nuclear Engineering Department for the education culminated by this thesis and their assistance during its preparation.

Finally, I would like to thank the Battelle Pacific Northwest Laboratories for sponsoring this research and providing the necessary financial support.

VIII. REFERENCES

Ah77 Ahmed, M., 1977, "A Comparative Study of n-γ Discrimination Properties of Scintillators NE 213, C_6H_6, C_6D_6 and Stilbene", Nucl. Instru. and Meths., 143, 255-257.

Al61 Alexander, T. K. and F. S. Goulding, 1961, "An Amplitude Insensitive System that Distinguishes Pulses of Different Shapes", Nucl. Instr. and Meths. 13, 244-246.

Bo72 Bovet, E., P. Boschung and J. Rossel, 1972, "Light Response and Pulse Shape Discrimination Properties for NE 232", Nucl. Instru. and Meths., 101, 315-319.

Ch84 Chilton, Arthur B., J. Kenneth Shultis, and Richard E. Faw, Principles of Radiation Shielding, (Prentice-Hall, Inc., Englewood Cliffs, New Jersey, 1984), pp. 70-73.

Cr83 Cross, W. G., 1983, private communication.

Ei85 Eisen, Y., B. H. Erkkila, R. J. Brake and W. P. Unruh, 1985, "A New Method for Measuring Beta Spectra and Doses in Mixed Beta-Photon Fields," Nucl. Instru. and Methods, A238, 187-190.

Er85 Erkkila, B. H., M. A. Wolf, Y. Eisen, W. P. Unruh, and R. J. Brake, 1985, "A Beta-Gamma Discrimination Circuit", IEEE Trans. Nucl. Sci. NS-32, No. 1, 969-971.

Ga62 Gatti, E. and F. De Martini, 1962, "A New Liner Method of Discrimination Between Elementary Particles in Scintillation Counters," Nuclear Electronics 2, I.A.E.A., Vienna, 265.

Ho67 Hollandsworth, C. E. and W. P. Bucher, 1967, "Wide-Range Pulse Shape Discrimination System", Rev. of Sci. Instru. 39, 2, 165-168.

Ka70 Kalyna, J. and I. J. Taylor, 1970, "Pulse Shape Discrimination: an Investigation of n-γ Discrimination with Respect to Size of Liquid Scintillator", Nucl. Instru. and Meths., 88, 277-287.

Kn79 Knoll, G. F., Radiation Detection and Measurement, (John Wiley & Sons, Inc., New York, 1979), pp. 152.

Sh72 Shoffner, B. M., 1972, "A Pulse Shape Analyzer for Phoswich Detectors", IEEE Trans. Nucl. Sci. NS-19, No. 1, 502-511.

Si82 Simons, G. G., T. M. DeBey, R. B. Stuewe and K. D. Stansbury, 1982, "Beta Dosimetry and Spectroscopy", Department of Nuclear Engineering, Annual Report to Battelle Pacific Northwest Laboratory.

Si85 Simons, G. G. and J. F. Higginbotham, 1985, "Beta Particle Spectroscopy with Active Gamma-ray Discrimination", Department of Nuclear Engineering, Kansas State University, Annual Report to Battelle Pacific Northwest Laboratory.

Sp74 Speer, P., H. Spieler, M. R. Maier and D. Evers, 1974, "A Simple Pulse-Shape Discrimination Circuit," Nucl. Instr. and Meths. 116, 55-59.

Sy72 Syme, D. B. C. B. and G. I. Crawford, 1972, "Pulse Shape Discrimination with NE211 Liquid Scintillator", Nucl. Instru. and Meths., 104, 245-247.

Ta70 Taylor, I. J. and J. Kalyna, 1970, "A High Speed Pulse Shape Discriminator," Nucl. Instru. and Meths., 88, 267-275.

Wi72 Winyard, R. A. and G. W. McBeth, 1972, "Pulse Shape Discrimination in Inorganic and Organic Scintillators, II", Nucl. Instru. and Methods, 98, 525-533.

PHOSWICH BETA-GAMMA SPECTROSCOPY

by

Allen Eugene Moon
B.S., Kansas State University, 1985

AN ABSTRACT OF
A MASTER'S THESIS

submitted in partial fulfillment of the
requirements for the degree

MASTER OF SCIENCE

Department of Nuclear Engineering
KANSAS STATE UNIVERSITY
Manhattan, Kansas

1987

ABSTRACT

There are many applications where it is desired to be able to accurately measure the separate beta particle and gamma ray components of a mixed beta-gamma radiation field. A well known passive discrimination technique involves taking a beta + gamma measurement, then covering the detector with a beta particle screen and taking a gamma only measurement. The gamma only measurement is then subtracted from the beta + gamma measurement, giving the beta particle result. However, this result has a large statistical error. The goal of this project was to study active beta-gamma discrimination using phoswich detector pulse shape discrimination.

The phoswich detector studied in this project consisted of a thin plastic scintillator having a long characteristic decay time placed atop of a thick plastic scintillator having a short characteristic decay time. Theoretical equations were derived to predict the performance of a phoswich detector beta-gamma spectroscopy system. Theoretical calculations showed the importance of controlling the amount of light reaching the photocathode of the PMT from each scintillator. Phoswich detector design chracteristics studied were gamma discrimination ratio, optimum thickness of each scintillator, and distortions in the linearity between absorbed beta particle energy and assigned channel number by a MCA. The theoretical output voltage waveforms produced by commercial pulse shape discrimination circuitry were compared with laboratory measured

waveforms. The results confirm the validity and usefulness of these theoretical calculations.